

Modeling Nearly Spherical Pure-Bulge Galaxies with a Stellar Mass-to-Light Ratio Gradient under the Λ CDM and MOND Paradigms: I. Methodology, Dynamical Stellar Mass, and Fundamental Mass Plane

Kyu-Hyun Chae

Department of Physics and Astronomy, Sejong University, 209 Neungdong-ro Gwangjin-gu, Seoul 05006, Republic of Korea

chae@sejong.ac.kr

Mariangela Bernardi

Department of Physics and Astronomy, University of Pennsylvania, 209 South 33rd Street, Philadelphia, PA 19104, USA

bernardm@sas.upenn.edu

and

Ravi K. Sheth

Department of Physics and Astronomy, University of Pennsylvania, 209 South 33rd Street, Philadelphia, PA 19104, USA

shethrk@physics.upenn.edu

ABSTRACT

We carry out spherical Jeans modeling of nearly round pure-bulge galaxies selected from the ATLAS^{3D} sample. Our modeling allows for gradients in the stellar mass-to-light ratio (M_*/L) through analytic prescriptions parameterized with a “gradient strength” K introduced to accommodate any viable gradient. We use a generalized Osipkov-Merritt model for the velocity dispersion (VD) anisotropy. We produce Monte Carlo sets of models based on the stellar VD profiles under both the Λ CDM and MOND paradigms. Here, we describe the galaxy data, the empirical inputs, and the modeling procedures of obtaining the Monte Carlo sets. We then present the projected dynamical stellar mass, M_{*e} , within the effective radius R_e , and the fundamental mass plane (FMP) as a function of K . We find the scaling of the K -dependent mass with respect to the ATLAS^{3D} reported mass as: $\log_{10} [M_{*e}(K)/M_{*e}^{\text{A3D}}] = a' + b'K$ with $a' = -0.019 \pm 0.012$ and $b' = -0.18 \pm 0.02$ (Λ CDM), or $a' = -0.023 \pm 0.014$ and $b' = -0.23 \pm 0.03$ (MOND), for $0 \leq K < 1.5$. The FMP has coefficients consistent with the virial expectation and only the zero-point scales with K . The median value of K for the ATLAS^{3D} galaxies is $\langle K \rangle = 0.53_{-0.04}^{+0.05}$. We perform a similar analysis of the much larger SDSS DR7 spectroscopic sample. In this case, only the VD within a single aperture is available, so we impose the additional requirement that the VD slope be similar to that in the ATLAS^{3D} galaxies. Our analysis of the SDSS galaxies suggests a positive correlation of K with stellar mass.

Subject headings: dark matter — galaxies: elliptical and lenticular — galaxies: kinematics and dynamics — galaxies: structure — gravitation

1. Introduction

Galaxies are fascinating objects in their own right as basic building blocks of the universe, but they also provide crucial laboratories for cosmology and fundamental physics. A main goal of cosmology is to understand how galaxies form and evolve (Mo, van den Bosch & White 2010) and observed stellar kinematics in galaxies (Binney & Tremaine 2008) provide evidence for unknown matter, referred to as dark matter (DM), or a new nature of gravity (Famaey & McGaugh 2012).

Galaxies exhibit great varieties in morphological appearance, constituents, kinematics, and dynamics, etc. From the viewpoint of kinematics and dynamics, galaxies can be broadly divided into two classes: rotationally-supported versus pressure(dispersion)-supported. In reality, most galaxies have multiple components often containing both rotating and non-rotating components. For example, most spiral or disk galaxies contain non-rotating central bulges and most early-type (i.e. elliptical and lenticular) galaxies contain rotating disks (Cappellari 2016).

In recent studies, it has been shown that rotating galaxies of various types satisfy Kepler-like kinematic laws such as the baryonic Tully-Fisher relation (McGaugh 2005) and the mass discrepancy-acceleration relation (or, radial acceleration relation) (McGaugh 2004; McGaugh, Lelli & Schombert 2016; Lelli et al. 2017). Considering the potentially profound physical implications of the radial acceleration relation (see, e.g., Famaey, Khoury & Penco 2018), it is interesting to explore whether there exists a universal radial acceleration relation for all galaxies, including non-rotating galaxies. In this respect, pure-bulge galaxies without rotating disks are of interest. These galaxies are also interesting for galactic astrophysics, e.g., as they may have been produced by the merging of galaxies, including rotating galaxies.

In this and companion/subsequent papers we analyze pure-bulge galaxies that also appear nearly round in projection. These galaxies form an extreme subset that is clearly distinct from other galaxies containing rotating components. One goal of studying these galaxies is to obtain an independent radial acceleration relation to compare with that of rotating galaxies and test theories of DM and gravity. The other goal is to model nearly spherical galaxies with a stellar mass-to-light ratio (M_*/L) gradient included, as motivated from recent empirical findings (Martín-Navarro et al. 2015; van Dokkum et al. 2017; Sonnenfeld et al. 2018) and quantify the effects of a M_*/L gradient on dynamical estimates of stellar masses, VD anisotropy, and galactic structure.

We use 24 ATLAS^{3D} galaxies with observed VD maps and 4201 SDSS galaxies with measured aperture VDs. We obtain Monte Carlo sets of models through the spherical Jeans equation based on the VD maps (or aperture VDs) and other empirical inputs under both the Lambda cold DM (Λ CDM ; see, e.g., Mo, van den Bosch & White 2010) and modified Newtonian dynamics (MOND; Milgrom 1983) paradigms. Here we describe the data, the required empirical inputs and the modeling procedures. We then discuss dynamical estimate of stellar masses and the fundamental mass plane (FMP) in this paper. The radial acceleration relation based on the Monte Carlo sets is discussed in Chae, Bernardi & Sheth (2018) while the effects of M_*/L gradient on VD anisotropy, stellar, DM and total mass profiles, DM mass fraction, and MOND interpolating function (IF) are discussed in subsequent publications.

2. Framework and Data

We use strictly pure-bulge (i.e. spheroidal), mostly round (i.e. nearly spherical) galaxies selected from the ATLAS^{3D} sample (Cappellari et al. 2011) and the SDSS DR7 spectroscopic sample (Abazajian et al.

2009). For our selected galaxies, the baryonic mass is primarily stellar – gas and dust are negligible. We carry out kinematic Jeans analyses based on three key pieces of data/information:

1. The observed projected light distribution (i.e. surface brightness) $I(R)$, with its deprojected volume distribution $\rho_L(r)$.
2. The stellar mass-to-light ratio (M_\star/L), $\Upsilon_\star(R) = \Sigma_\star(R)/I(R)$, where $\Sigma_\star(R)$ denotes the projected stellar mass density.
3. Line-of-sight (LOS) stellar velocity dispersions (VDs) at multiple radii, i.e. the radial profile $\sigma_{\text{los}}(R)$ for ATLAS^{3D} galaxies, or the mean value within an aperture radius R_{ap} , $\sigma_{\text{ap}} = \langle \sigma_{\text{los}} \rangle (R = R_{\text{ap}})$ (see below for details) for SDSS galaxies.

2.1. Stellar Mass-to-light Ratio Gradient

We use an empirically motivated stellar mass-to-light ratio radial gradient given by

$$\frac{\Upsilon_\star(R/R_e)}{\Upsilon_{\star 0}} = \max \{ 1 + K [A - B(R/R_e)], 1 \}, \quad (1)$$

where $(A, B) = (2.33, 6.00)$ are derived by Bernardi et al. (2018a) for the recently observed gradient (van Dokkum et al. 2017). The parameter K introduced here describes the gradient “strength”: $K = 0$, 1, and 0.555 correspond, respectively, to no gradient, the strong gradient (van Dokkum et al. 2017), and an intermediate gradient, i.e. the **Salp**^{In}-**Chab**^{Out} model in which the stellar initial mass function (IMF) varies from the heavy Salpeter (1955) IMF in the center to the light Chabrier (2003) IMF in the outer region (Bernardi et al. 2018a). We consider the range $0 \leq K < 1.5$ to encompass all likely possibilities.

2.2. Spherical Jeans Equation

For a spherical galaxy with $\Sigma_\star(R) = \Upsilon_\star(R/R_e)I(R)$ from which the baryonic volume density $\rho_B(r)$ [= $\rho_\star(r)$ here] is obtained by deprojection, we solve the spherical Jeans equation (Binney & Tremaine 2008)

$$\frac{d[\rho_B(r)\sigma_r^2(r)]}{dr} + 2\frac{\beta(r)}{r}[\rho_B(r)\sigma_r^2(r)] = -\rho_B(r)a(r), \quad (2)$$

for the radial stellar VD $\sigma_r(r)$. Here, $a(r)$ is the gravitational acceleration (see §2.4). We assign a central black hole using a recent result (Saglia et al. 2016). In Equation (2) the anisotropy parameter $\beta(r) = 1 - \sigma_t^2(r)/\sigma_r^2(r)$ links the radial VD with the tangential VD $\sigma_t(r) \equiv \sqrt{[\sigma_\theta^2(r) + \sigma_\phi^2(r)]/2}$. We consider radially constant anisotropies and also radially varying anisotropies given by

$$\beta_{\text{gOM}}(r) = \beta_0 + (\beta_\infty - \beta_0)\frac{(r/r_a)^2}{1 + (r/r_a)^2}, \quad (3)$$

which varies smoothly from a central value β_0 to β_∞ at infinity. We refer to this model as a generalized Osipkov-Merritt (gOM) model (Binney & Tremaine 2008) since the combination of $\beta_0 = 0$ and $\beta_\infty = 1$ corresponds to the Osipkov-Merritt model (Osipkov 1979; Merritt 1985).

The observable LOSVD of stars at a projected radius R on the sky, $\sigma_{\text{los}}(R)$, is then given by (Binney & Mamon 1982)

$$I(R)\sigma_{\text{los}}^2(R) = 2 \int_R^\infty \rho_L(r)\sigma_r^2(r) \left[1 - \frac{R^2}{r^2}\beta(r) \right] \frac{rdr}{\sqrt{r^2 - R^2}}, \quad (4)$$

where we use light (rather than mass) densities $\rho_L(r)$ and $I(R)$ appropriate for the case of radially varying $\Upsilon_*(R)$ (Bernardi et al. 2018a). When aperture VDs are only available (but, radial profiles of LOSVDs are not), as is the case for SDSS galaxies, we will work with the light-weighted mean value of LOSVDs within a circular aperture:

$$\langle \sigma_{\text{los}} \rangle(R) \equiv \frac{\int_0^R I(R')\sigma_{\text{los}}(R')R'dR'}{\int_0^R I(R')R'dR'}, \quad (5)$$

where $\sigma_{\text{los}}(R')$ is given by Equation (4) and $I(R')$ is the surface brightness distribution.

2.3. Integral Solution of the Spherical Jeans Equation

For a given baryonic (stellar) mass density $\rho_B(r)$ with a model for gravitational acceleration $a(r)$ under the Λ CDM or the MOND paradigm, the solution of equation (2) for the radial stellar VD $\sigma_r(r)$ can be expressed, following appendix B of Chae et al. (2012), as

$$\sigma_r^2(r) = \int_r^\infty \frac{\omega(t)}{\omega(r)} \frac{\rho_B(t)}{\rho_B(r)} a(t) dt, \quad (6)$$

where $\omega(r) = \exp \left[\int^r (2\beta(r')/r') dr' \right]$ for an anisotropy $\beta(r')$ (Equation 3). This integral can be evaluated numerically. Typically it is sufficient to replace the infinite upper bound with $\sim 30 R_e$. Examples of using this integral equation for the Λ CDM and the MOND paradigm can be found in Chae, Bernardi & Kravtsov (2014) and Chae & Gong (2015).

2.4. Gravitational Acceleration

For a galaxy with (observationally inferred) baryonic mass volume density $\rho_B(r)$ the gravitational acceleration at r depends on the assumed paradigm, i.e. Λ CDM or MOND. Under the Λ CDM paradigm we assume that the baryonic mass distribution is embedded in an extended DM mass distribution $\rho_{\text{DM}}(r)$ (see §2.5). Then, the gravitational acceleration is given by

$$a(r) = G \frac{M_B(r) + M_{\text{DM}}(r)}{r^2}, \quad (7)$$

where $M_B(r)$ and $M_{\text{DM}}(r)$ are the integrated masses within r for $\rho_B(r)$ and $\rho_{\text{DM}}(r)$, respectively.

Under the MOND paradigm the gravitational acceleration is given by

$$a(r) = f \left(\frac{a_B(r)}{a_0} \right) a_B(r) \quad \text{with} \quad a_B(r) = G \frac{M_B(r)}{r^2}, \quad (8)$$

where $a_B(r)$ is the Newtonian acceleration predicted by the distribution of baryons. In Equation (8) $f(x)$ is known as an IF (see §2.6) and a_0 is a free parameter known as the critical (or, characteristic) acceleration fitted to the data. The IF satisfies the limiting behaviors $f(x) \rightarrow 1$ for $x \equiv a_B/a_0 \gg 1$ and $f(x) \rightarrow \sqrt{a_0/a_B}$ for $x \ll 1$, which means that only below a_0 does the empirical acceleration $a(r)$ deviate substantially from the Newtonian prediction $a_B(r)$.

2.5. Empirical Constraints on Dark Halos

Our analysis under the Λ CDM paradigm assumes that a spherical dark halo embeds each pure-bulge galaxy under consideration. To describe the unknown DM mass distribution we use the NFW model (Navarro, Frenk & White 1997) suggested from N -body simulations of CDM, but with its density slope parameter allowed to vary from the CDM-only prediction, so that possible effects of galaxy formation and evolution (Mo, van den Bosch & White 2010) can be mimicked. A generalized NFW (gNFW) model is described by

$$\rho_{\text{gNFW}}(r) \propto r^{-\alpha} \left[1 + c_{200} \left(\frac{r}{r_{200}} \right) \right]^{-3+\alpha}, \quad (9)$$

where inner slope α and concentration c_{200} are allowed to vary from the NFW values $\alpha_{\text{NFW}} = 1$ and c_{NFW} . In Equation (9), r_{200} denotes the radius of the sphere within which the DM density is 200 times the cosmic mean matter density. For a halo at redshift z , the radius r_{200} is given by

$$r_{200} = \frac{162.7}{1+z} \left(\frac{M_{200}}{10^{12} M_{\odot}/h} \right)^{1/3} h^{-1} \Omega_{\text{m}0}^{-1/3} \text{ kpc}, \quad (10)$$

where M_{200} is the integrated mass of the halo within r_{200} , $h = H_0/100 \text{ km s}^{-1} \text{ Mpc}^{-1}$ is the normalized Hubble constant, and $\Omega_{\text{m}0} = \rho_{\text{m}0}/\rho_{\text{crit}0} = \rho_{\text{m}0}/[3H_0^2/(8\pi G)]$ is the cosmic mean matter density normalized by the critical density $\rho_{\text{crit}0} = 3H_0^2/(8\pi G)$ at $z = 0$.

The weak-lensing study by Mandelbaum et al. (2016) presents a numerical relation between M_{200} and M_{\star}^{Krou} (their Table B1) where M_{\star}^{Krou} is the total stellar mass of the galaxy estimated for the Kroupa (Kroupa 2002) IMF. Our fiducial choice of M_{\star}^{Krou} is their MPA-JHU value. The difference between their MPA-JHU and VAGC values is ~ 0.09 dex for $M_{\star}^{\text{Krou}} \sim 10^{11} M_{\odot}$. This uncertainty in M_{\star}^{Krou} and the measurement uncertainty of ~ 0.05 dex in M_{200} give rise to a total uncertainty of ~ 0.2 dex in M_{200} because $\log_{10} M_{\star}^{\text{Krou}} \sim 2 \log_{10} M_{200} + \text{const}$. Figure 1 shows the relation with the estimated uncertainties. It also shows alternative relations, including that based on satellite kinematics (More et al. 2011), that are within the displayed uncertainties.

We also use a recent N -body prediction of the M_{200} - c_{NFW} correlation (Diemer & Kravtsov 2015), which is consistent with weak-lensing constraint (Mandelbaum, Seljak & Hirata 2008), and impose the constraint that the DM profile mimics the NFW profile for $r > 0.2r_{200}$, consistent with weak-lensing empirical results (Mandelbaum, Seljak & Hirata 2008; Mandelbaum et al. 2016). By doing so we are excluding unlikely wild combinations of α and c_{200} . For this we follow the simple procedure described in Section 3.3.1 of Chae, Bernardi & Kravtsov (2014).

2.6. MOND IF

For the MOND IF defined in Equation (8) we use the family of models indexed by ν ,

$$f_{\nu}(x) = \left(\frac{1}{2} + \sqrt{\frac{1}{4} + \frac{1}{x^{\nu}}} \right)^{1/\nu}, \quad (11)$$

where $\nu = 1$ is the ‘simple’ (Famaey & Binney 2005) and $\nu = 2$ is the ‘standard’ case (Kent 1987). We consider $0 < \nu \leq 2$, which can encompass various possibilities suggested in the literature. See Chae, Bernardi & Sheth (2018) for other functional forms.

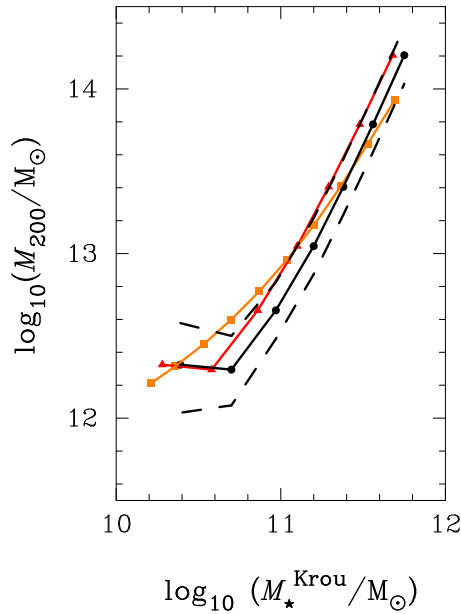


Fig. 1.— Empirical stellar mass(M_{\star}^{Krou})–halo mass(M_{200}) relation used in this work under the DM paradigm. Here, M_{\star}^{Krou} denotes the stellar mass for the Kroupa (2002) IMF, while M_{200} denotes the mass within a spherical halo whose mean density is 200 times the cosmic mean matter density. The black solid and dashed curves represent, respectively, the weak-lensing relation by Mandelbaum et al. (2016) and our uncertainties (estimated including stellar mass uncertainties) based on their MPA-JHU stellar masses. The red triangles and curve are for their VAGC stellar masses. The orange squares and curve represent the relation from satellite kinematics by More et al. (2011).

2.7. ATLAS^{3D} Galaxies

2.7.1. Light Distribution, Mass-to-light Ratio Gradient, and Stellar Mass Distribution

The ATLAS^{3D} team (Scott et al. 2013) describes the 2-dimensional distribution of light (i.e. surface brightness) using the so-called multi-Gaussian expansion (MGE) model (Emsellem, Monnet & Bacon 1994):

$$I(X, Y) = \sum_{j=1}^N I'_j \exp \left[-\frac{1}{2\sigma_j^2} \left(X^2 + \frac{Y^2}{q_j'^2} \right) \right], \quad (12)$$

where parameters I'_j , σ_j , and q'_j can be found from the ATLAS^{3D} project website (<http://www-astro.physics.ox.ac.uk/atlas3d/>). The luminosity based on the MGE model is given by

$$L_{\text{MGE}} = \sum_{j=1}^N 2\pi I'_j \sigma_j^2 q'_j. \quad (13)$$

This is likely to be an underestimate of the true total luminosity because the expansion terms typically do not include light at large radii ($\gtrsim 2 - 3 R_e$), and there is no extrapolation term to estimate light at large radii. For the same reason the half-light radius ($R_{e,\text{MGE}}$) based on Equations (12) and (13) is smaller than the true value R_e . In fact, the ATLAS^{3D} team reports $R_e = 1.35 R_{e,\text{MGE}}$ (Cappellari et al. 2013a). We

estimate the projected light within R_e using an MGE light distribution of $\approx 0.594L_{\text{MGE}}$, from which we estimate the total luminosity as $L_{\text{tot}} \approx 1.188L_{\text{MGE}}$.

In this work we only consider nearly round pure-bulge galaxies under the spherical symmetry assumption. We thus circularize the observed light distribution with the substitution ($\sigma_j \rightarrow \sigma_j \sqrt{q'_j}$, $q'_j \rightarrow 1$), following, e.g. Cappellari et al. (2013a), as

$$I(R) = \sum_{j=1}^N I'_j \exp\left(-\frac{1}{2\sigma_j^2 q'_j} R^2\right), \quad (14)$$

where $R = \sqrt{X^2 + Y^2}$ is the radius on the sky. The integrated light within R on the 2-dimensional plane is then given by

$$L^{2\text{D}}(R) = 2\pi \sum_{j=1}^N I'_j \sigma_j^2 q'_j \left[1 - \exp\left(-\frac{1}{2\sigma_j^2 q'_j} R^2\right)\right]. \quad (15)$$

Deprojecting the 2-dimensional circular light distribution (Equation 14) yields

$$\rho_{\text{L}}(r) = \sum_{j=1}^N I'_j \sqrt{\frac{1}{2\pi\sigma_j^2 q'_j}} \exp\left(-\frac{1}{2\sigma_j^2 q'_j} r^2\right), \quad (16)$$

where r is the three-dimensional (rather than projected) radius. The integrated light within r in the 3-dimensional space is then given by

$$L^{3\text{D}}(r) = 2\pi \sum_{j=1}^N I'_j \sigma_j^2 q'_j \left[\text{erf}\left(\sqrt{k_j} r\right) - 2\sqrt{\frac{k_j}{\pi}} r \exp(-k_j r^2)\right], \quad (17)$$

where $k_j \equiv 1/(2\sigma_j^2 q'_j)$ and $\text{erf}(x)$ is the error function.

If the stellar mass-to-light ratio were constant (denoted by $\Upsilon_{\star 0}$) throughout a galaxy, then the stellar mass density $\rho_{\star}(r)$ would simply be equal to Equation (17) multiplied by $\Upsilon_{\star 0}$. For radially varying $\Upsilon_{\star}(R)$ the projected stellar mass density can be written by

$$\Sigma_{\star}(R) = \Upsilon_{\star}(R)I(R) = \Upsilon_{\star 0} \frac{\Upsilon_{\star}(R)}{\Upsilon_{\star 0}} I(R) = \Upsilon_{\star 0} \tilde{I}(R), \quad (18)$$

where $\Upsilon_{\star 0}$ is a constant representing M_{\star}/L for $R > 0.4R_e$ (cf. Equation 1) and we have defined an effective light distribution $\tilde{I}(R) \equiv [\Upsilon_{\star}(R)/\Upsilon_{\star 0}] I(R)$. For $\Upsilon_{\star}(R)/\Upsilon_{\star 0}$ given by Equation (1), deprojection of $\Sigma_{\star}(R)$ [or $\tilde{I}(R)$] may be cumbersome. Instead of considering the direct deprojection, we rescale the coefficients $I'_j \rightarrow \tilde{I}'_j$ using a prescription given by

$$\tilde{I}'_j = I'_j \times \max\{1 + K[-1 + f_0 + f_1(\sigma_j/R_e)], 1\}, \quad (19)$$

where K is the gradient strength defined in Equation (1) and parameters f_0 and f_1 are fitted for each galaxy. For example, NGC 5557 has $f_0 = 3.745$ and $f_1 = -6.594$ determined for $K = 1$. Then, the effective distribution $\tilde{I}(R)$ in Equation (18) can be approximated by

$$\tilde{I}(R) = \sum_{j=1}^N \tilde{I}'_j \exp\left(-\frac{1}{2\sigma_j^2 q'_j} R^2\right). \quad (20)$$

Figure 2 shows the observed light distribution $I(R)$, the effective distribution given by Equation (18), and the distribution given by Equation (20) fitted with Equation (19) for NGC 5557. One can see that the fitted

distribution matches well the effective distribution for most radial range, but not near the transition radius $0.4R_e$. Actually, the fitted distribution even appears to be preferable, as it varies more smoothly in the transition region.

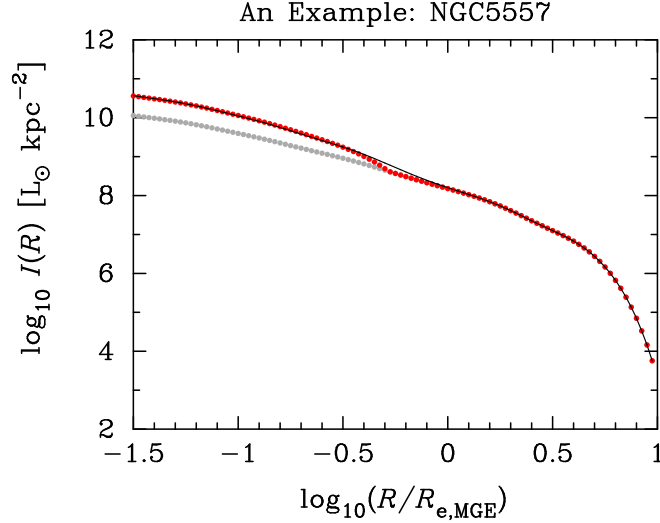


Fig. 2.— Observed surface brightness distribution described by the MGE model (gray) and the effective distribution (red) defined by multiplying $\Upsilon_*(R)/\Upsilon_{*0}$ (Equation 1 with $K = 1$) by the observed distribution. The black curve fitted to red dots is the modified MGE model (Equation 20) with the modified coefficients defined by Equation (19).

Based on the above, the projected stellar mass density can be approximated by

$$\Sigma_*(R) = \Upsilon_{*0} \tilde{I}(R) = \Upsilon_{*0} \sum_{j=1}^N \tilde{I}'_j \exp\left(-\frac{1}{2\sigma_j'^2 q_j'} R^2\right), \quad (21)$$

where the \tilde{I}'_j are the effective coefficients given by Equation (19). The volume stellar mass density needed for the Jeans equation (Equation 2) is then

$$\rho_B(r) = \Upsilon_{*0} \sum_{j=1}^N \tilde{I}'_j \sqrt{\frac{1}{2\pi\sigma_j'^2 q_j'}} \exp\left(-\frac{1}{2\sigma_j'^2 q_j'} r^2\right), \quad (22)$$

and the baryonic (stellar) integrated mass within r is given by

$$M_B(r) = 2\pi\Upsilon_{*0} \sum_{j=1}^N \tilde{I}'_j \sigma_j'^2 q_j' \left[\operatorname{erf}\left(\sqrt{k_j} r\right) - 2\sqrt{\frac{k_j}{\pi}} r \exp(-k_j r^2) \right]. \quad (23)$$

Note that Equations (22) and (23) can be, respectively, obtained by multiplying Equations (16) and (17) by Υ_{*0} with the replacement of $I_j \rightarrow I'_j$ (Equation 19).

2.7.2. Selection of Pure-bulge Galaxies and Their VD Profiles

The vast majority of the 260 ATLAS^{3D} galaxies possess some rotation (Emsellem et al. 2011). This means that only a small fraction of the ATLAS^{3D} galaxies can be included in our selection of (little-rotating) pure-bulge galaxies, for which the spherical Jeans equation applies. Our selection of pure-bulge galaxies is based on a photometric analysis by Krajnović et al. (2013) who decomposed the observed light distribution into two components, a disk described by an exponential profile and a bulge described by a Sérsic profile for galaxies that do not possess bars. They report the relative amounts of light contained in the two components. We only take galaxies for which a disk is not detected at all or the measured light in the disk is less than 5% of the total light, and the reported Sérsic index $n > 3$ (to make sure that the bulge is clearly different from the disk profile). This resulted in the following 27 galaxies: NGC 0661 ($n = 5.4$), NGC 1289 (4.3), NGC 2695 (5.2), NGC 3182 (3.5), NGC 3193 (5.0), NGC 3607 (4.7), NGC 4261 (4.4), NGC 4365 (4.3), NGC 4374 (5.0), NGC 4406 (3.6), NGC 4459 (4.3), NGC 4472 (4.7), NGC 4486 (4.2), NGC 4636 (3.8), NGC 4753 (2.9), NGC 5322 (4.6), NGC 5481 (4.2), NGC 5485 (3.7), NGC 5557 (4.6), NGC 5631 (4.9), NGC 5831 (3.9), NGC 5846 (3.5), NGC 5869 (5.2), NGC 6703 (4.7) and NGC 0680 (7.6), NGC 4552 (7.3), NGC 5576 (8.3). The values provided in parentheses are our estimates of the Sérsic index by fitting the observed light distributions with fixed $R_e = 1.35R_{e,\text{MGE}}$. An example of such fits can be found in Figure 3. We also fitted these galaxies with a constraint $n < n_{\text{max}}$ with R_e allowed to be free. In this case we find that the fitted R_e matches $1.35R_{e,\text{MGE}}$ only for $n_{\text{max}} \leq 5.5$. As n gets larger than 5.5, the fitted R_e becomes increasingly larger than $1.35R_{e,\text{MGE}}$. This raises potential problems in using $R_e = 1.35R_{e,\text{MGE}}$ for galaxies with $n > 5.5$ as we use $R_e = 1.35R_{e,\text{MGE}}$ throughout, particularly in deriving the FMP for pure-bulge galaxies. To avoid any biases we thus exclude the last three galaxies in the list above – NGC 0 680, NGC 4552, and NGC 5576 – from our analysis. The final 24 pure-bulge galaxies have accurate light distributions up to $\sim 2 - 3R_e$ described by the MGE model and the well-understood R_e using the extrapolated Sérsic light profiles.

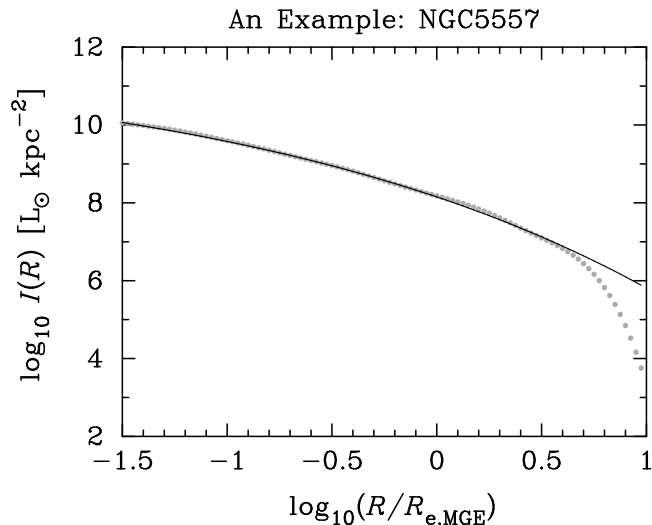


Fig. 3.— Example of fitting the observed surface brightness distribution described by the MGE model (gray dots) with the Sérsic model (black curve) with the constraint $R_e = 1.35R_{e,\text{MGE}}$. Note that the ATLAS^{3D} provided MGE distribution declines rapidly well outside R_e due to the absence of higher-order terms.

Our photometrically defined pure-bulge ATLAS^{3D} galaxies are nearly round, with a mean minor-to-

major axis ratio of $\langle b/a \rangle = 0.82$. Nearly round galaxies with a low disk-to-total light ratio (D/T) and large Sérsic index $n > 3$ are expected to be little-rotating (Krajinović et al. 2013). Indeed, the selected 24 pure-bulges are overall consistent with kinematic identifications. Based on the angular momentum parameter λ_{R_e} within R_e (Table B1, Emsellem et al. (2011)), 16 (67%) out of the 24 pure-bulges are classified as slow rotators. Our Jeans analysis is little affected whether we exclude the 8 kinematically fast rotators or not. We will use all 24 (photometrically identified) pure-bulges for our analyses.

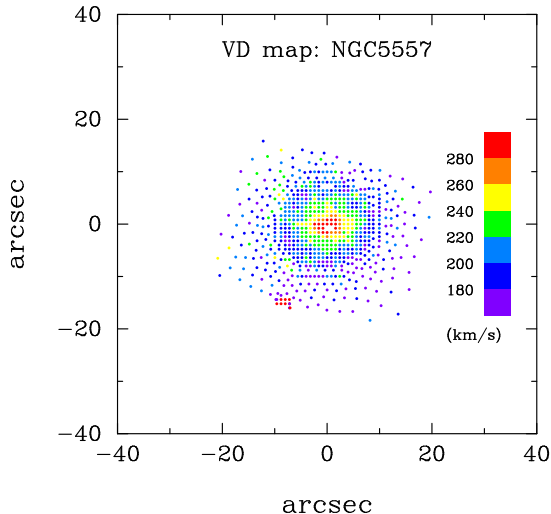


Fig. 4.— Example of the two-dimensional map of observed LOSVDs that has an approximate circular symmetry.

The ATLAS^{3D} galaxies have detailed maps of LOSVDs up to $\sim 1R_e$ which are exhibited in Cappellari et al. (2013a). An example is reproduced in Figure 4 using the public data for NGC 5557 obtained from the project page. This figure contains 692 data points. We construct a radial VD profile using the data points. Figure 5 exhibits the distribution of the measured VDs with radius for NGC 5557. To construct a VD profile the observed radial range is divided into radial bins so that each bin contains at least 21 VDs. Using the VDs in each bin we calculate the statistically weighted mean (or the median) and the 68% scatter from which we estimate the uncertainty of the mean assuming the normal distribution in the bin. Figure 5 shows the constructed VDP of NGC5557 for which each bin contains 21 data points except for the last bin. Figure 6 exhibits the VDPs for all 24 pure-bulge galaxies.

2.8. SDSS Galaxies

2.8.1. SDSS Pure-bulge Galaxies: Sample Selection

The final data release of SDSS I (DR7) provides light distributions and spectra for nearly one million galaxies (Abazajian et al. 2009). The enormous sample size is useful for addressing many science issues, including the radial acceleration relation and galactic structure. However, SDSS galaxy spectra were obtained using a fixed aperture radius of $\theta_{\text{ap}} = 1.5$ arcsec. This means that the SDSS aperture VD σ_{ap} equals $\langle \sigma_{\text{los}} \rangle (R_{\text{ap}})$ of Equation (5), where $R_{\text{ap}} = \theta_{\text{ap}} D$ and D is the distance to each galaxy. We convert from

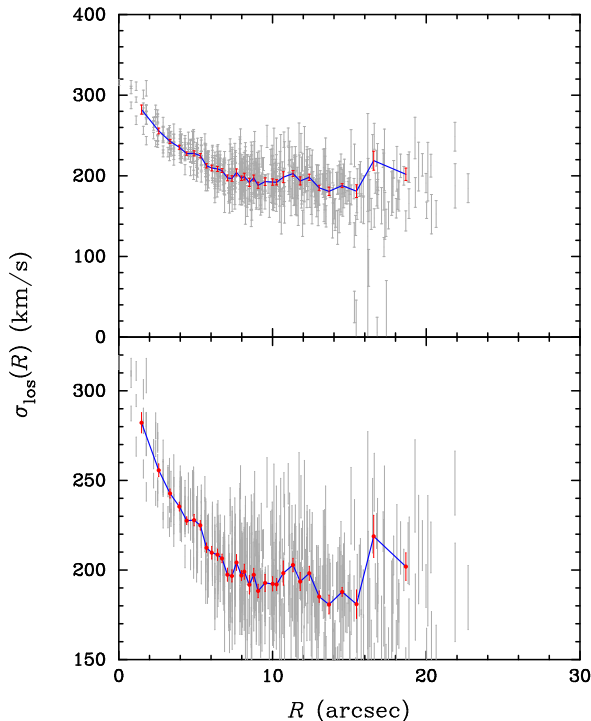


Fig. 5.— Radial profile of LOSVDs constructed using the VD map of Figure 4. Radial bins are formed by concentric rings in the VD map so that each ring except for the last ring contains 21 VDs. The gray points and bars represent the measured VDs and uncertainties. The red points with error bars are the weighted means, with their uncertainties estimated by the 68% scatters divided by $\sqrt{(N - 1)}$. The bottom panel is a zoomed-in view magnified vertically.

the measured redshift z to the distance D using a flat Λ CDM cosmological model with the present matter density of $\Omega_{m0} = 0.3$ and the Hubble constant of $H_0 = 70 \text{ km s}^{-1} \text{ Mpc}^{-1}$.

With σ_{ap} measured at a single scale only, rather than a VD profile $\sigma_{\text{los}}(R)$ over a range of scales, M_*/L and DM distribution (or MOND IF) cannot be well constrained by the SDSS data alone. Therefore, we use an FMP derived from ATLAS^{3D} pure-bulge galaxies (see §3.2) to provide an additional empirical constraint.

We draw pure-bulge, round galaxies from the UPENN database of ≈ 0.7 million galaxies (http://www.physics.upenn.edu/~ameert/SDSS_PhotDec/) for which light distributions have been thoroughly analyzed (Meert, Vikram & Bernardi 2015). For most of these galaxies the aperture VDs have been reliably derived by two groups (MPA-JHU, Portsmouth) (see <http://www.sdss.org/dr12/spectro/galaxy/> and also Thomas et al. (2013) for the Portsmouth VDs). We select pure-bulge galaxies using flag bit 2 in the UPENN catalog and further require that galaxies have probabilities of being elliptical of greater than 70% using an automated morphological classification (Huertas-Company et al. 2001) to exclude lenticular galaxies seen face-on by chance. To select round galaxies we require a minor-to-major axis ratio > 0.85 . These are conservative cuts that are satisfied by only $\approx 11,000$ galaxies. Of these, we only retain those galaxies whose photometric measurements (R_e and radial light profile) and subsequent FMP-based estimate of stellar mass density are robust. For this we require SDSS r -band absolute magnitude $M_r > -23$ (to exclude too bright and large galaxies), stellar mass $M_* > 10^{10.4} M_\odot$ (here M_* refers to the FMP-based value), and

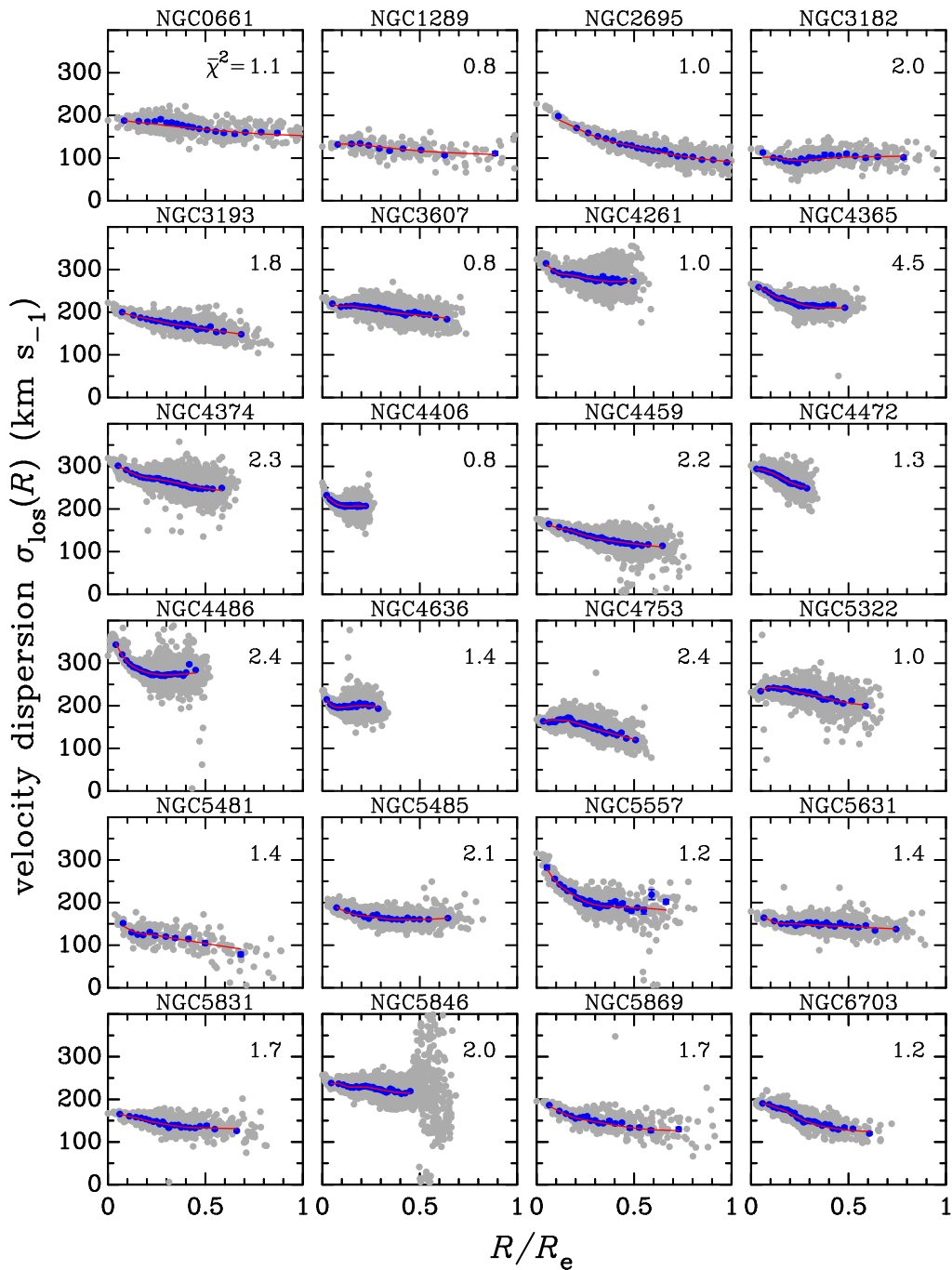


Fig. 6.— Line-of-sight velocity dispersion profiles of 24 pure-bulge ATLAS^{3D} galaxies. The gray points are the measured values on the sky distributed with radius. The blue points represent the weighted means in radial bins, each bin containing at least 21 measurements. Each red curve represents the prediction by the best-fit model for the galaxy with the gNFW DM halo (Equation 9) and the gOM anisotropy (Equation 3). The best-fit reduced chi-squared $\bar{\chi}^2 \approx \chi^2/N_{\text{bins}}$ value is given in each panel. Modeling under the MOND paradigm gives similar fit results.

Sérsic index $3 < n < 5.5$, where the lower cut is to ensure light profiles well distinct from disk galaxies and the upper cut is to ensure that the Sérsic-based R_e matches the ATLAS^{3D} reported R_e . This upper cut matters because we are using the FMP relation that is derived using the ATLAS^{3D} reported R_e values. Lastly, we use only those galaxies whose measured VDs have uncertainties smaller than 1/3 of the values (but, typical uncertainties are small, just 0.02–0.04 dex). Our final sample contains 4201 (4229) galaxies for MPA-JHU (Portsmouth) VDs. The typical difference between the two VDs is 0.02 dex (or 5%) which shows a good agreement between the two. We will use the MPA-JHU VDs throughout, but with their formal errors multiplied by $\sqrt{2}$, considering the small difference with the Portsmouth VDs.

2.8.2. *SDSS Pure-bulge Galaxies: Statistical Properties and Implicit Stacking*

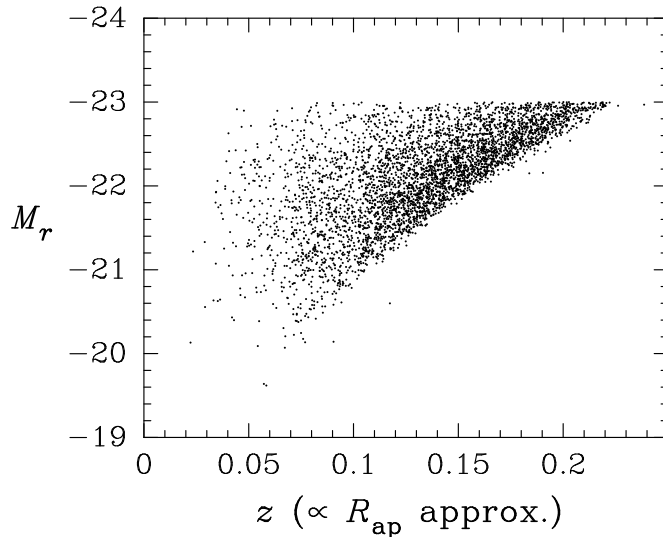


Fig. 7.— Distribution of 4201 nearly round pure-bulge SDSS galaxies in the redshift(z)-absolute magnitude(M_r) plane, where M_r is the absolute magnitude in the SDSS r -band. Because SDSS used a fixed spectroscopic aperture radius of 1.5 arcsec, at fixed M_r galaxies of different redshifts have aperture VDs within different projected aperture radii, R_{ap} that is approximately scaling linearly with z for the shown redshift range.

Figure 7 shows the distribution of galaxies in the redshift(z)-absolute magnitude(M_r) plane. At low redshift ($z \lesssim 0.2$) the angular-diameter distance to a galaxy increases approximately linearly with z so that the physical aperture radius R_{ap} for a fixed angular radius $\theta_{\text{ap}} = 1.5$ arcsec is approximately proportional to z . Thus, many galaxies of the same luminosity have different values of R_{ap} providing a stacked profile of $\sigma_{\text{ap}}(R_{\text{ap}})$ at fixed M_r , something similar to the observed LOSVD profile $\sigma_{\text{los}}(R)$ in ATLAS^{3D} galaxies. We can construct a better stacked profile of $\sigma_{\text{ap}}(R_{\text{ap}})$ using additional galaxy parameters. For example, we can construct $\sigma_{\text{ap}}(R_{\text{ap}})$ at fixed M_r , R_e and n . This stacking is implicit in our analysis based on SDSS galaxies. In other words, although each galaxy uses just one value of the aperture VD at R_{ap} , those values can be attributed to certain stacked profiles.

2.8.3. Double-Gaussian Model to Represent the Stellar Mass-to-light Ratio Gradient for the Sérsic Light Profile

Unlike the MGE model in which its own parameters can be adjusted to accommodate the effect of a M_*/L gradient, the Sérsic light profile does not allow such a flexibility because it has only two parameters to describe the shape, i.e., n and R_e . It is convenient to represent the effect of a M_*/L gradient in the central region using an analytically tractable double-Gaussian model written as

$$I_{\text{cen}}(R) = I_{\text{cen},1} \exp\left(-\frac{R^2}{2\sigma_{\text{cen},1}^2}\right) + I_{\text{cen},2} \exp\left(-\frac{R^2}{2\sigma_{\text{cen},2}^2}\right), \quad (24)$$

whose total luminosity is $L_{\text{cen}} = 2\pi(I_{\text{cen},1}\sigma_{\text{cen},1}^2 + I_{\text{cen},2}\sigma_{\text{cen},2}^2)$. The deprojected volume density is given by

$$\rho_{L,\text{cen}}(r) = \frac{I_{\text{cen},1}}{\sqrt{2\pi\sigma_{\text{cen},1}^2}} \exp\left(-\frac{r^2}{2\sigma_{\text{cen},1}^2}\right) + \frac{I_{\text{cen},2}}{\sqrt{2\pi\sigma_{\text{cen},2}^2}} \exp\left(-\frac{r^2}{2\sigma_{\text{cen},2}^2}\right), \quad (25)$$

and the integrated luminosity within r is given by

$$L_{\text{cen}}(r) = 2\pi \sum_{j=1}^2 I_{\text{cen},j} \sigma_{\text{cen},j}^2 \left[\text{erf}\left(\frac{r}{\sqrt{2}\sigma_{\text{cen},j}}\right) - \sqrt{\frac{2}{\pi\sigma_{\text{cen},j}^2}} r \exp\left(-\frac{r^2}{2\sigma_{\text{cen},j}^2}\right) \right]. \quad (26)$$

For the light distribution described by a Sérsic light profile $I_{\text{Ser}}(R)$ and the radially varying stellar mass-to-light ratio $\Upsilon_*(R)$ (Equation 1), the projected stellar mass density (see Equation 18) can be approximated as follows:

$$\Sigma_*(R) = \Upsilon_*(R)I_{\text{Ser}}(R) = \Upsilon_{*0}\tilde{I}_{\text{Ser}}(R) \simeq \Upsilon_{*0}[I_{\text{Ser}}(R) + I_{\text{cen}}(R)], \quad (27)$$

where $I_{\text{cen}}(R)$ is the added central component given by Equation (24) to represent the gradient, and $\tilde{I}_{\text{Ser}}(R) \simeq I_{\text{Ser}}(R) + I_{\text{cen}}(R)$ is the effective distribution as if the ratio were a constant Υ_{*0} .

For the gradient model under consideration (Equation 1) we can set $I_{\text{cen},2} = 0.3I_{\text{cen},1}$ and $\sigma_{\text{cen},2} = 3.3\sigma_{\text{cen},1}$ based on numerical investigation. So we rewrite Equation (24) as

$$I_{\text{cen}}(R) = I_{\text{cen}} \left[\exp\left(-\frac{R^2}{2R_{\text{cen}}^2}\right) + 0.3 \exp\left(-\frac{R^2}{2(3.3R_{\text{cen}})^2}\right) \right] \quad (28)$$

with $L_{\text{cen}} = 8.534\pi I_{\text{cen}} R_{\text{cen}}^2$, which now has just two free parameters R_{cen} and L_{cen} (or I_{cen}). Let $F_{\text{cen}} \equiv L_{\text{cen}}/L_{\text{Ser}}$ where L_{Ser} is the total luminosity of the Sérsic light distribution. Then, we can solve numerically Equation (27) to find the best-fit F_{cen} and R_{cen} for a given Sérsic profile. Figure 8 shows an example with gradient strength $K = 1$ for a Sérsic index $n = 4.635$. From numerical results at various values of n we find

$$F_{\text{cen}}(n) = 0.31091 + 0.02813(n - 4) - 0.00331(n - 4)^2, \quad (29)$$

and

$$R_{\text{cen}}(n) = 0.03976 - 0.00675(n - 4) + 0.00143(n - 4)^2 \quad (30)$$

in units of R_e for the range $3 \leq n \leq 5.5$ with $K = 1$. With other values of K , $R_{\text{cen}}(n)$ remains unchanged and $F_{\text{cen}}(n)|_K = K \times F_{\text{cen}}(n)|_{K=1}$, to a good approximation. Figure 9 shows numerical examples fitted with these curves.

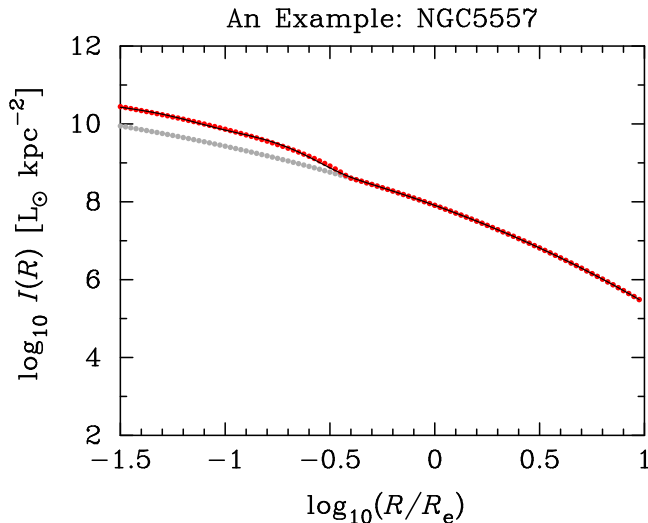


Fig. 8.— Example of the Sérsic profile with $n = 4.635$ (gray dots), fitted to the MGE surface brightness distribution of NGC 5557 (Fig. 3), and the effective distribution (red dots) defined by multiplying $\Upsilon_*(R)/\Upsilon_{*0}$ (Equation 1 with $K = 1$) by the Sérsic function. The black curve fitted to the red dots is the composite distribution that includes an added double-Gaussian model (Equation 28) to accommodate the central radial gradient.

The total stellar mass for the distribution of Equation (27) is

$$M_\star = \Upsilon_{*0}(L_{\text{Ser}} + L_{\text{cen}}) = M_{\star\text{Ser}} + M_{\star\text{cen}} = (1 + F_{\text{cen}})M_{\star\text{Ser}}, \quad (31)$$

where we define $M_{\star\text{Ser}} \equiv \Upsilon_{*0}L_{\text{Ser}}$ and $M_{\star\text{cen}} \equiv \Upsilon_{*0}L_{\text{cen}}$. The projected mass within the half-light radius R_e is then given by

$$M_{\star e} = \frac{1}{2}M_{\star\text{Ser}} + M_{\star\text{cen}} = \frac{1 + 2F_{\text{cen}}}{2(1 + F_{\text{cen}})}M_\star, \quad (32)$$

which is $> 0.5M_\star$ for $F_{\text{cen}} > 0$. The projected stellar mass density within R_e , $\mu_{\star e} \equiv M_{\star e}/(\pi R_e^2)$, is related to M_\star as follows:

$$\log_{10} M_\star = \log_{10} \mu_{\star e} + \log_{10}(2\pi R_e^2) - \log_{10} \left(\frac{1 + 2F_{\text{cen}}}{1 + F_{\text{cen}}} \right). \quad (33)$$

For a SDSS pure-bulge galaxy with its measured n , R_e and σ_e we can estimate M_\star (or Υ_{*0}) and mass densities using the FMP derived for the ATLAS^{3D} galaxies as a function of K . We first estimate $\mu_{\star e}$ using the FMP as a function of K (see §3.2). We estimate $F_{\text{cen}}(n)$ as a function of K and $R_{\text{cen}}(n)$ independent of K as described above. With the set $\{\mu_{\star e}, F_{\text{cen}}(n), R_{\text{cen}}(n)\}$ we can estimate M_\star using Equation (33) and then the projected density (Equation 27), the volume density and the stellar mass within a spherical radius with Equations (24)—(26) for the central component and with the corresponding equations for the Sérsic body found in the literature (e.g., Appendix A of Chae et al. (2012)). Figure 10 shows an example of the deprojected 3-dimensional light distributions using NGC 5557. It shows the deprojected profiles of the observed surface brightness distribution and the effective distribution accommodating a central M_\star/L gradient using two approaches, i.e. the MGE model with effective coefficients (§2.7.1) and the Sérsic plus central double-Gaussian model considered in this section. These two approaches give overall consistent

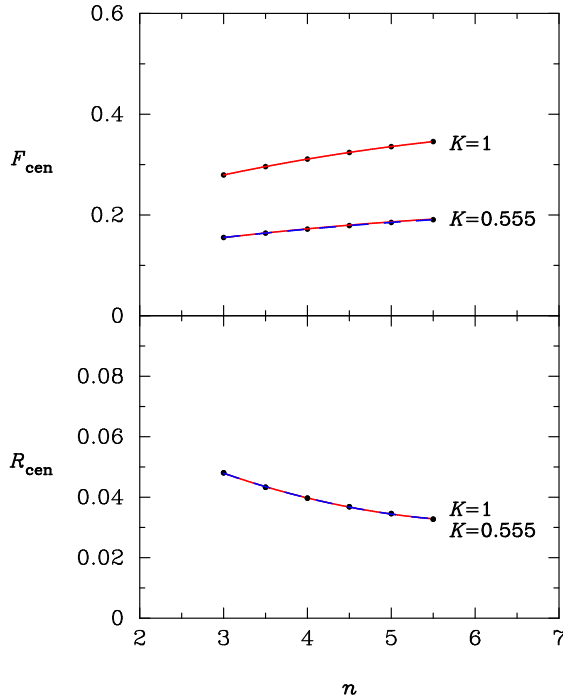


Fig. 9.— Relative mass (F_{cen}) and the relative core size of the first Gaussian component (R_{cen}) of the central double-Gaussian model compared with the main Sérsic body, numerically derived as a function of Sérsic index n for gradient strength $K = 1$ and 0.555 . At fixed n , $F_{\text{cen}}(K) = K \times F_{\text{cen}}(K = 1)$ to a good approximation as shown by the red and blue dashed curves at $K = 0.555$ where the blue curve represents the numerical fit results and the red curve is the prediction by $F_{\text{cen}}(K = 0.555) = 0.555 \times F_{\text{cen}}(K = 1)$. At fixed n , R_{cen} (in units of R_e) is independent of K to a good approximation. See the text for further details about the central double-Gaussian component.

results. Some minor discrepancies between the two, particularly near $0.4R_e$ have no impact on this work because the current large uncertainties in the M_*/L gradient do not warrant a very precise model.

3. Modeling Procedures and Results

Our goal is to construct Monte Carlo sets of models for baryonic and DM mass distributions under the Λ CDM paradigm, or for baryonic mass distribution plus MOND IF under the MOND paradigm. We derive a Monte Carlo set of models for each galaxy using the measured light distribution, a range of M_*/L gradients, and the measured VD profile for the ATLAS^{3D} galaxies, or the aperture VD for the SDSS galaxies. We consider the ATLAS^{3D} galaxies first and then the SDSS galaxies. In modeling the SDSS galaxies we use an FMP relation based on the modeling results for the ATLAS^{3D} galaxies.

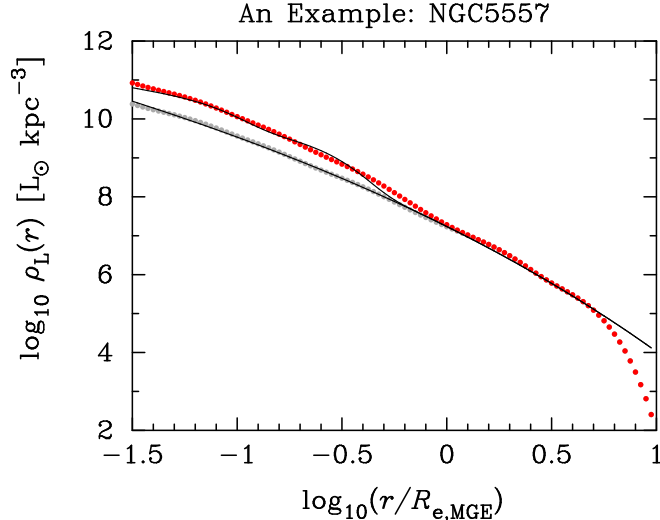


Fig. 10.— Example of the volume light distributions obtained by deprojecting the observed and the effective (i.e. accommodating M_*/L gradient in the central region) surface brightness distributions through two approaches. The gray and red dots represent the results through the MGE model, i.e. the deprojection of Figure 2, while the black curves represent the results through the Sérsic model with the added double-Gaussian model, i.e. the deprojection of Figure 8.

3.1. For the ATLAS^{3D} Galaxies

We use the VDP constructed from the measured LOSVD map as described in §2.7.2. Each radial bin at radius R_i contains at least 21 LOSVDs from which we obtain the statistically weighted mean (or median) $\sigma_{\text{los}}^{\text{obs}}(R_i)$ and the standard uncertainty s_i . We fit $\Upsilon_*(R)$ and the DM mass distribution $M_{\text{DM}}(r)$, or MOND IF, by minimizing the ‘goodness-of-fit’ statistic chi-squared

$$\chi^2 = \sum_{i=1}^{N_{\text{bin}}} \frac{[\sigma_{\text{los}}^{\text{obs}}(R_i) - \sigma_{\text{los}}(R = R_i)]^2}{s_i^2}, \quad (34)$$

where $\sigma_{\text{los}}(R = R_i)$ is the LOSVD (Equation 4) predicted by the model under consideration.

To obtain a Monte Carlo set of models for each galaxy under the Λ CDM paradigm, we first draw DM halo parameters $\{M_{200}, c_{\text{NFW}}, \alpha\}$. For halo mass M_{200} we take a Gaussian deviate of $\log_{10} M_{200}$ using its empirical correlation with a fixed IMF-based stellar mass with a typical scatter of ~ 0.2 dex (§2.5, Figure 1). For c_{NFW} we take a Gaussian deviate using $c_{\text{NFW}} = (7.192/(1+z))(M_{200}/(10^{14}M_{\odot}/h))^{-\varepsilon}$, where z is the redshift of the galaxy, $h = 0.7$ and $\varepsilon = 0.114$, with an rms scatter of 0.15. For the profile slope α we take a uniform deviate from the range $0 < \alpha < 1.8$. Note that c_{200} follows from α and c_{NFW} using the weak-lensing constraint for $r > 0.2r_{200}$ (see §2.5). We also take a M_*/L gradient strength K from $0 \leq K < 1.5$. For the MOND case we draw ν (Equation 11) from $0 < \nu \leq 2$ and a_0 from $0.5 < a_0/(10^{-10}\text{m s}^{-2}) < 1.9$. For each random draw of $\{M_{200}, c_{\text{NFW}}, \alpha, K\}$ or $\{\nu, a_0, K\}$, Υ_{*0} and the given anisotropy model are varied to minimize χ^2 . Anisotropy values are allowed to vary between -2 and 0.7 so that the ratio σ_t^2/σ_r^2 varies between $1/3$ and 3 .

For a good model we expect the reduced chi-squared $\bar{\chi}^2 = \chi^2/N_{\text{dof}} \sim 1$ where the degree of freedom

$N_{\text{dof}} = N_{\text{bin}} - N_{\text{free}} \approx N_{\text{bin}}$ which is typically 20–30. With constant anisotropies, good fits ($\bar{\chi}^2 \lesssim 2$) cannot be found for about 40% of galaxies. With varying gOM anisotropies (Equation 3) good fits ($\bar{\chi}^2 \lesssim 2$) are found for most galaxies. Figure 11 shows a detailed example of successful models with $\bar{\chi}^2 \sim 1$ overplotted on the observed VDP of NGC 5557 for the Λ CDM case. Figure 11 also illustrates the unsuccessful prediction without DM. Figure 6 exhibits the formal best-fit (i.e. $\bar{\chi}^2 = \bar{\chi}_{\text{min}}^2$) models for all 24 ATLAS^{3D} pure-bulges for the Λ CDM case. Very similar results are obtained for the MOND case as well.

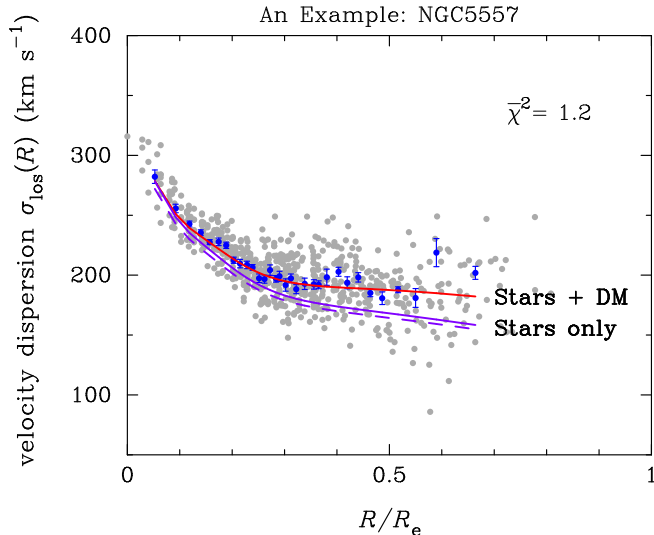


Fig. 11.— Example of the observed LOSVDs and their successful modeling under the Λ CDM paradigm. The gray dots are individual measurements on the sky and blue dots represent binned, error-weighted means. The red curve is the prediction by the successful model which has a reduced chi-squared of $\bar{\chi}^2 = 1.2$. The purple dashed curve is the prediction by the stellar mass distribution only. The purple solid curve is the readjusted prediction by the stellar mass distribution so that the innermost VDs are reproduced.

For each galaxy, 800 Monte Carlo models are produced within the prior parameter ranges. But we keep only those models with $\bar{\chi}^2 < 2\bar{\chi}_{\text{min}}^2$ where $\bar{\chi}_{\text{min}}^2$ is the minimum value obtained for the best-fit model. Using these models we calculate the likely range of M_*/L gradient strength K , stellar masses, and the FMP, which are described below. In companion and subsequent papers we use the sets to investigate the likely ranges of mass profiles, DM fractions, MOND IFs, VD anisotropies, and the radial acceleration relation.

Figure 12 shows the distributions of K from the models satisfying $\bar{\chi}^2 < 2\bar{\chi}_{\text{min}}^2$ for all 24 galaxies. There are significant galaxy-to-galaxy scatters for K . There are also severe degeneracies of K in many cases (e.g. NGC 5557, NGC 5869, NGC 6703 in particular). Due to these degeneracies and numerical limitations, best-fit and median values of K are sometimes discrepant. Considering the degeneracies the median values are more likely to be meaningful. Figure 13 exhibits the distribution of the medians and the averaged probability density of K based on the individual distributions of Figure 12. The distribution of the median values is peaked near $\langle K \rangle = 0.5$. We estimate $\langle K \rangle = 0.53_{-0.04}^{+0.05}$ along with an rms scatter of $s_K = 0.17_{-0.03}^{+0.06}$ based on a bootstrap method using the distribution. This value is lower than the null result 0.75 (recall that our prior range is $0 \leq K < 1.5$). The distribution of the averaged probability density is tilted from the horizontal line showing that a strong gradient ($K \gtrsim 1$) is less likely. This result agrees well with the intermediate strength $K = 0.555$ suggested by Bernardi et al. (2018a), which is weaker than the van Dokkum et al. (2017) strength

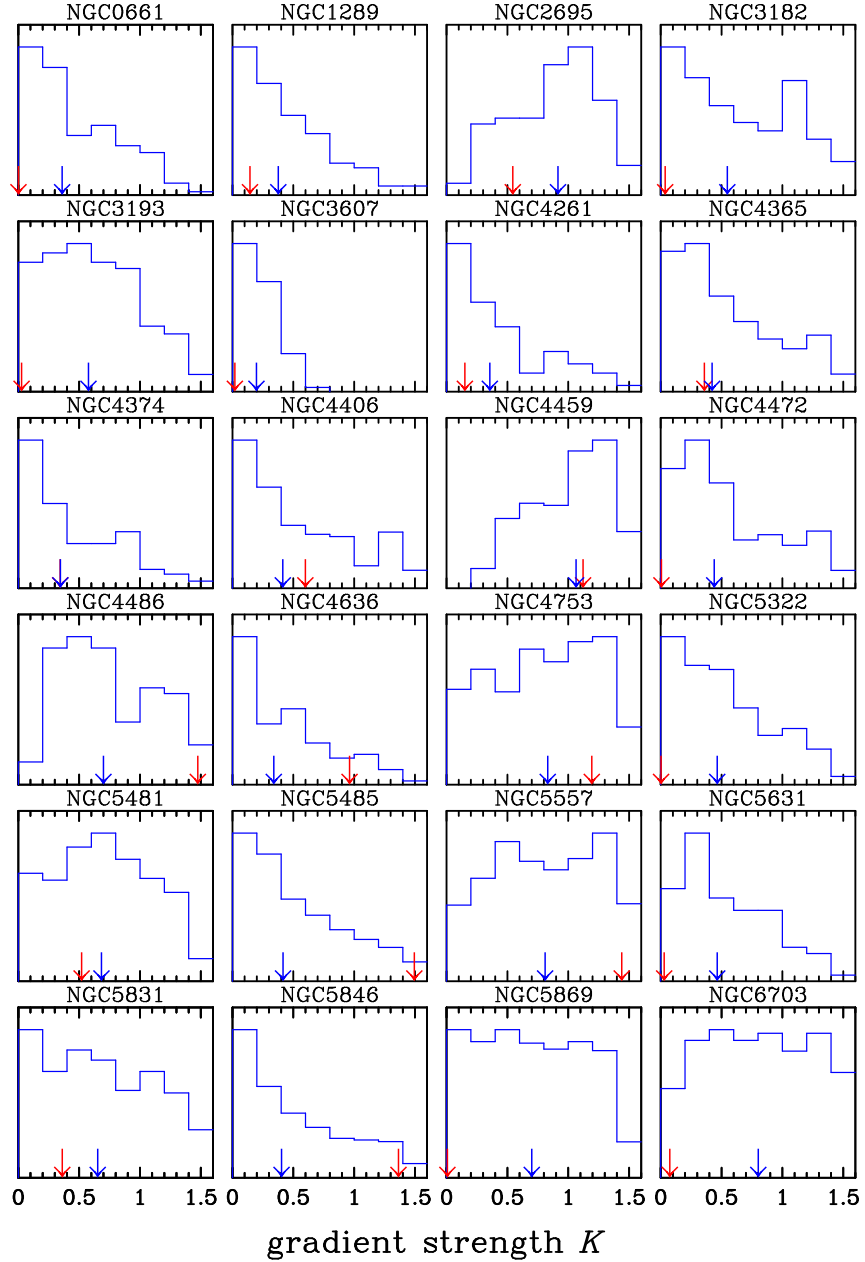


Fig. 12.— Histograms showing distributions of M_*/L gradient strength K (Equation 1) from the Monte Carlo sets of models satisfying $\bar{\chi}^2 < 2\bar{\chi}_{\min}^2$ for the ATLAS^{3D} galaxies shown in Fig. 6. The red arrows indicate best-fit values (i.e. for the best-fit models satisfying $\bar{\chi}^2 = \bar{\chi}_{\min}^2$), while the blue arrows indicate median values from the models.

$K = 1$. Very similar results are obtained under the MOND paradigm, as shown in Figure 14.

3.2. The FMP Relation with a Stellar Mass-to-light Ratio Gradient

Elliptical galaxies are supposed to be in dynamical equilibrium. According to the virial theorem (Binney & Tremaine 2008) we expect correlations between a fiducial radius (which is chosen to be R_e here), dynamical total mass ($M_{\text{dyn},e}$), and an observable mean VD squared (σ_e^2 is a proxy for mean kinetic energy), both within that radius: $M_{\text{dyn},e}/R_e \propto \sigma_e^2$. Let $M_{\star e}$ be the projected stellar mass within R_e . Then we expect a good correlation between $M_{\star e}$ and $M_{\text{dyn},e}$, and hence we expect the following correlation

$$w = a + b(x - x_0) + c(y - y_0), \quad (35)$$

where $x \equiv \log_{10} \sigma_e$, $y \equiv \log_{10} R_e$ and $w \equiv \log_{10} \mu_{\star e} = \log_{10} [M_{\star e}/(\pi R_e^2)]$. Equation (35) is a representation of the fundamental plane of early-type galaxies (Djorgovski & Davis 1987; Dressler et al. 1987). (Here σ_e is in km s^{-1} , R_e is in kpc, and mass density is in $M_\odot \text{kpc}^{-2}$.) We take R_e and σ_e (the aperture VD within R_e) from Cappellari et al. (2013a). For a case with a constant stellar mass-to-light ratio (denoted by $\Upsilon_{\star 0}$), we estimate $M_{\star e}$ using an empirical relation $M_{\star e} \approx 0.594 M_{\star \text{MGE}}$ derived for the 24 pure-bulge galaxies, where $M_{\star \text{MGE}}$ is the analytic stellar mass for the MGE distribution, i.e. $M_{\star \text{MGE}} = \Upsilon_{\star 0} L_{\text{MGE}}$. Here, we can take $\Upsilon_{\star 0}$ and L_{MGE} from the ATLAS^{3D} reported results (Cappellari et al. 2013a,b). We can also estimate $M_{\star e}$ using our Monte Carlo sets, which are based on radially varying anisotropies (Equation 3). Note that the ATLAS^{3D} modeling was based on radially constant anisotropies, although they used oblate spheroids rather than spherical models. The two results agree, as shown in Figure 15, although there are individual scatters.

Our derivation of the parameters of the plane is based on Equation (7) of Cappellari et al. (2013a). Namely, we minimize the quantity

$$\Delta^2 = \sum_{j=1}^{N_{\text{gal}}} \frac{[a + b(x_j - x_0) + c(y_j - y_0) - w_j]^2}{(bs_{x_j})^2 + (cs_{y_j})^2 + (s_{w_j})^2 + \varepsilon_w^2}, \quad (36)$$

where $x_0 = 2.11$ and $y_0 = 0.301$, as in Cappellari et al. (2013a), s_{x_j} and s_{y_j} are the ATLAS^{3D} reported errors and s_{w_j} is estimated using the standard error propagation, assuming normal errors. In Equation (36), ε_w is the intrinsic scatter of w that is estimated so that the minimized Δ^2 is equal to $N_{\text{gal}} - 4$ (degree of freedom). We estimate the errors of the parameters a , b , and c by generating Monte Carlo sets of data $\mathcal{D}^{(i)} = \{x_j^{(i)}, y_j^{(i)}, w_j^{(i)}\}$ ($j = 1, \dots, N_{\text{gal}}$) and obtaining $\{a^{(i)}, b^{(i)}, c^{(i)}\}$ fitted to $\mathcal{D}^{(i)}$ ($i = 1, \dots, 900$).

For the case of constant M_\star/L [$K = 0$ in Equation (1)] the FMP parameter values obtained for all ATLAS^{3D} galaxies (except for two galaxies for which not all necessary galaxy parameter values are provided) are $a = 9.174 \pm 0.007$, $b = 2.22 \pm 0.05$, $c = -1.13 \pm 0.04$ (with $\varepsilon_w = 0.088$), and an rms scatter of $\Delta_w = 0.145$. For the 24 pure-bulge galaxies we have $a = 9.141 \pm 0.058$, $b = 2.27 \pm 0.34$, $c = -1.05 \pm 0.21$ (with $\varepsilon_w = 0$), and $\Delta_w = 0.062$. These two results are consistent with each other and the virial expectation, i.e. $b = 2$ and $c = -1$. Figure 16 shows this explicitly: the two FMP estimates of w_j given the measured x_j and y_j are very similar. Our estimate of the FMP is also similar to that reported in Cappellari et al. (2013a), based on a dynamical mass M_{JAM} that is obtained by multiplying their dynamical (stellar plus dark) mass-to-light ratio by their total luminosity; their reported parameters in their Figure 12 (second panel) can be translated to $a = 9.197 \pm 0.004$, $b = 1.928 \pm 0.026$, and $c = -1.036 \pm 0.018$ if we use $M_{\text{JAM}}/(2\pi R_e^2)$ as a proxy for $\mu_{\star e}$.

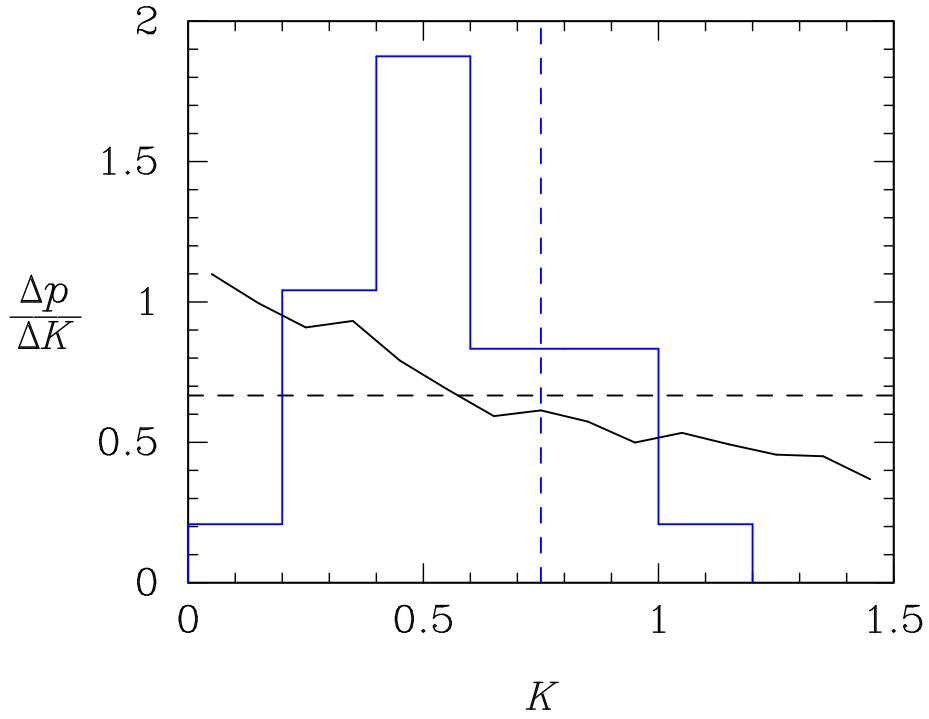


Fig. 13.— Probability distribution of K values for the 24 ATLAS^{3D} galaxies shown in Figure 12. The black solid curve is the averaged distribution of the individual distributions, while the horizontal dashed line is the expected null result. The blue histogram represents the distribution of the individual medians, while the vertical dashed line is the expected null result. These results show that a strong gradient ($K \gtrsim 1$) is less likely.

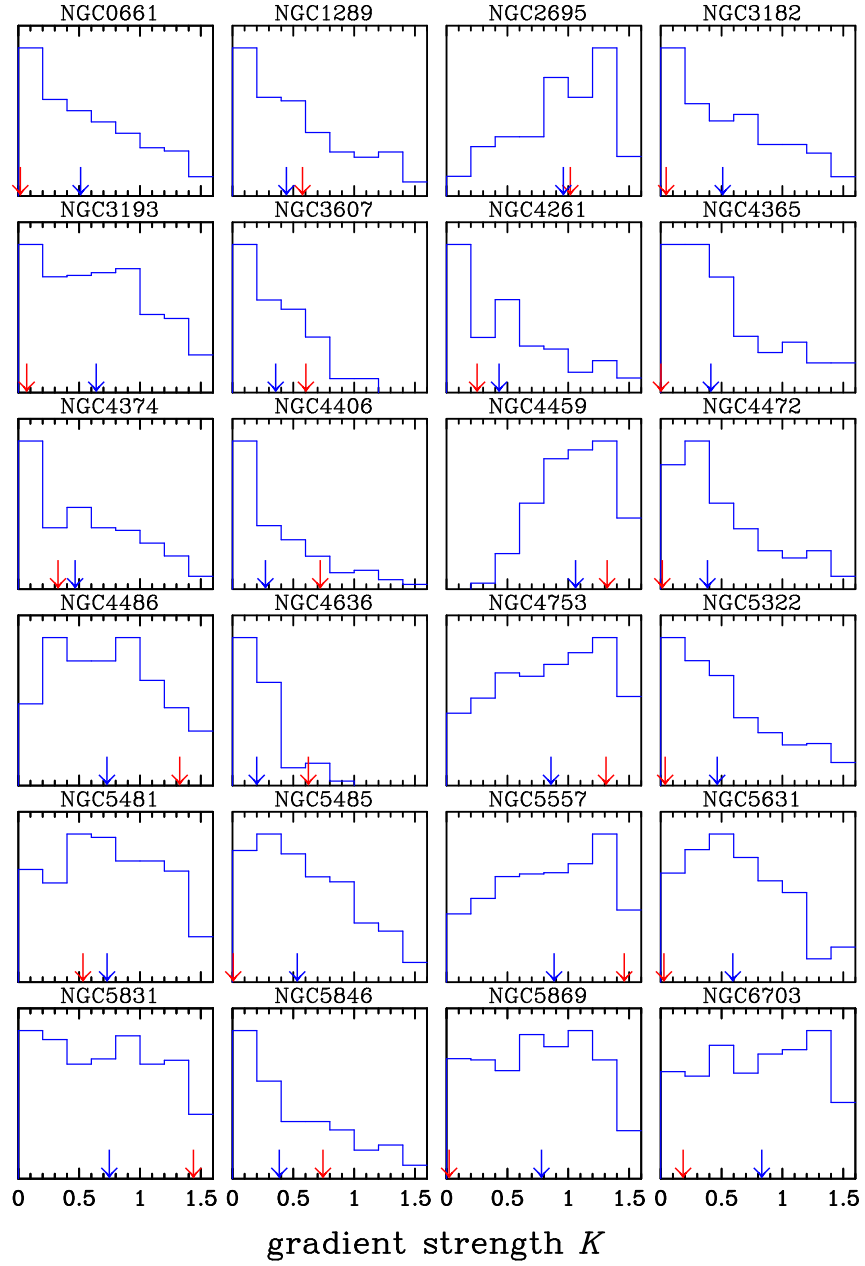


Fig. 14.— Same as Figure 12 but under the MOND paradigm.

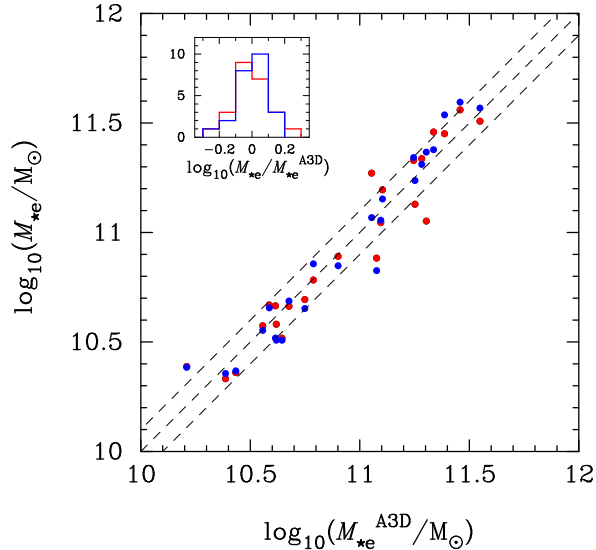


Fig. 15.— Consistency of the projected stellar mass within R_e between the ATLAS^{3D} reported values and our modeling results for the 24 pure-bulge galaxies under the Λ CDM paradigm, with the assumption of constant M_*/L . The red points represent the results for the best-fit models ($\bar{\chi}^2 = \bar{\chi}_{\min}^2$), while the blue points represent the median results for the models satisfying $\bar{\chi}^2 < 2\bar{\chi}_{\min}^2$.

The pure-bulge FMP allows an accurate estimate of M_{*e} for pure-bulge galaxies with measured σ_e and R_e under the assumption of constant M_*/L . If there is a M_*/L gradient ($K \neq 0$), we expect a systematic shift of M_{*e} as demonstrated in Bernardi et al. (2018a). We estimate the systematic shift with K using our Monte Carlo sets with $K \neq 0$ as shown in Figure 17. We find a linear relation $\log_{10} [M_{*e}(K)/M_{*e}^{\text{A3D}}] = a' + b'K$ with $a' = -0.024 \pm 0.013$ and $b' = -0.21 \pm 0.02$ (for the best-fit models), or $a' = -0.019 \pm 0.012$ and $b' = -0.18 \pm 0.02$ (for the median models), under the Λ CDM paradigm, where M_{*e}^{A3D} is from the ATLAS^{3D} (Cappellari et al. 2013a,b) modeling results. We obtain similar results (Figure 18) with respect to our own estimate of the mass at $K = 0$ as follows: $\log_{10} [M_{*e}(K)/M_{*e}(K = 0)] = a' + b'K$ with $a' = -0.014 \pm 0.010$ and $b' = -0.20 \pm 0.02$ (for the best-fit models), or $a' = -0.011 \pm 0.011$ and $b' = -0.20 \pm 0.02$ (for the median models). Under the MOND paradigm the corresponding results are as follows, as shown in Figures 19 and 20: $a' = 0.010 \pm 0.015$ and $b' = -0.25 \pm 0.03$ (for the best-fit models), or $a' = -0.023 \pm 0.014$ and $b' = -0.23 \pm 0.03$ (for the median models), with respect to M_{*e}^{A3D} ; and, $a' = 0.014 \pm 0.018$ and $b' = -0.25 \pm 0.03$ (for the best-fit models), or $a' = 0.002 \pm 0.012$ and $b' = -0.26 \pm 0.03$ (for the median models), with respect to $M_{*e}(K = 0)$. The above results, with respect to M_{*e}^{A3D} , are consistent with $a' = 0$, again confirming the consistency between our results for $K = 0$ and the ATLAS^{3D} results. Regarding the slope b' the Λ CDM results give $b' \approx -0.20$, while the MOND results give ≈ -0.05 dex shifted values with larger uncertainties.

We use the median relations to correct the parameter a of the FMP when $K \neq 0$ while keeping b and c fixed:

$$a(K) = a(K = 0) + b'K \quad (37)$$

where $b' = -0.18 \pm 0.02$ (Λ CDM) or -0.23 ± 0.03 (MOND). There are always some trade-offs among a , b , and c when fitting the plane for real (imperfect) data. Hence, whether fixing b and c at the values for $K = 0$

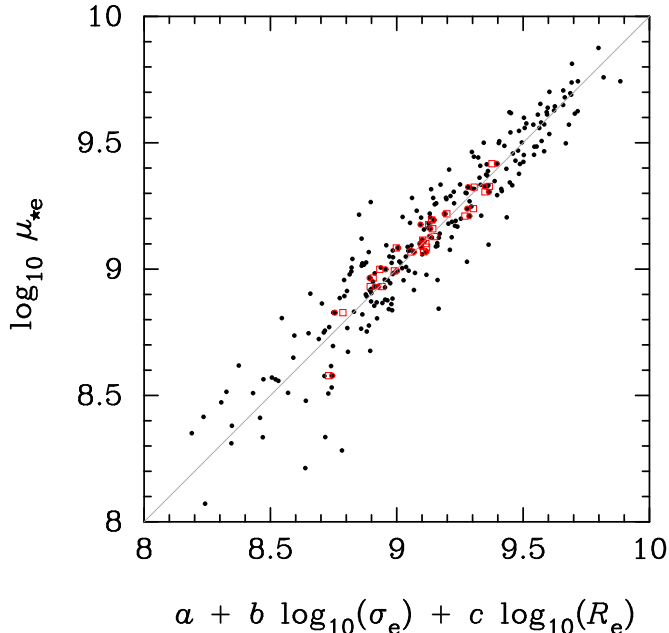


Fig. 16.— Fundamental mass plane (FMP) relation for ATLAS^{3D} galaxies among $\log_{10}(\sigma_e)$, $\log_{10}(R_e)$ and $\log_{10} \mu_{*e} \equiv \log_{10}[M_{*e}/(\pi R_e^2)]$. Here, σ_e is in km s^{-1} , R_e is in kpc, and M_{*e} is in M_\odot (solar masses). For the zero-points of $\log_{10}(\sigma_e)$ and $\log_{10}(R_e)$ we take $x_0 = 2.11$ and $y_0 = 0.301$. The black dots represent 258 ATLAS^{3D} early-type galaxies. The black dots within red circles are 24 pure-bulge galaxies. The open red squares represent the FMP derived only for the pure-bulges.

or allowing them to be free makes little difference about the plane for $K \neq 0$. For the sake of simplicity we fix b and c while allowing only a to vary with K .

The above results suggest that dynamical estimates of stellar masses with the van Dokkum et al. (2017) M_*/L gradient would be ≈ -0.2 dex shifted from that with constant M_*/L . This shift is ≈ 0.1 dex lesser than an estimate with isotropic velocity dispersions for all galaxies (Bernardi et al. 2018a). This is because in fitting the observed VDPs galaxies with larger gradients, $\langle K \rangle$, requires lower values of VD anisotropy $\langle \beta_e \rangle$ (Figure 21), where β_e is the radially averaged anisotropy within R_e , i.e.,

$$\beta_e \equiv \frac{1}{R_e} \int_0^{R_e} \beta(r) dr. \quad (38)$$

This systematic variation of the fitted $\langle \beta_e \rangle$ with $\langle K \rangle$ had a systematic impact on the scaling of Equation (37), weakening the slope b' because the predicted VDP at fixed K depends on VD anisotropy, as illustrated in Figure 2 of Bernardi et al. (2018a) using radially constant anisotropies.

3.3. For the SDSS Galaxies

For each SDSS galaxy with a measured geometric property (i.e. Sérsic parameters, n and R_e) and kinematic property (i.e. aperture VD, σ_{ap}) we start by generating 90 Monte Carlo sets of $(R_e, n, w = \log_{10} \mu_{*e})$, where $\mu_{*e} = M_{*e}(K = 0)/(\pi R_e^2)$ is the projected stellar mass density when there is no M_*/L

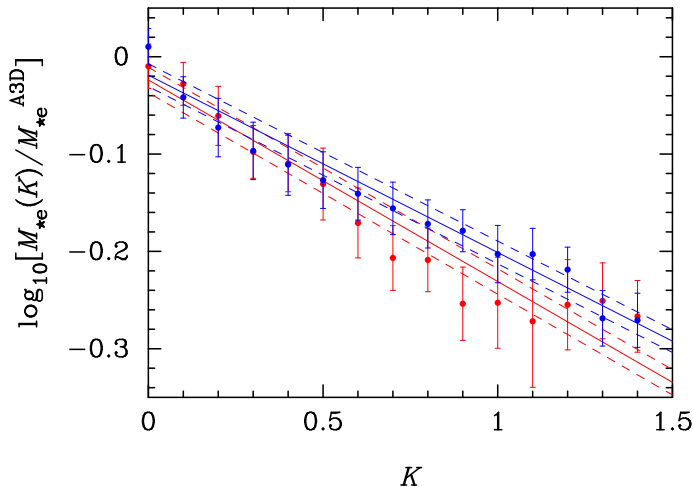


Fig. 17.— Dependence of the dynamical estimate of the projected stellar mass within R_e (M_{*e}) on M_*/L gradient strength (K) in the 24 pure-bulge ATLAS^{3D} galaxies. Here, M_{*e} is the estimate as a function of K based on our Jeans modeling results under the Λ CDM paradigm, whereas M_{*e}^{A3D} is the estimate based on the ATLAS^{3D} JAM modeling results for $K = 0$. The red and blue points represent the results, respectively, for the best-fit and the median models. The solid lines are the least-square fit results. The dashed lines represent the uncertainties of the y-intercept. The fit results are as follows: $y = a' + b'K$ with $a' = -0.024 \pm 0.013$ and $b' = -0.21 \pm 0.02$ (red, best-fit), or $a' = -0.019 \pm 0.012$ and $b' = -0.18 \pm 0.02$ (blue, median).

gradient. Parameters R_e and n are generated from a bi-variate Gaussian distribution with their measurement errors and a correlation coefficient of $\rho_{R_e, n} = 0.07$ (Meert, Vikram & Bernardi 2013). Parameter w is generated from a Gaussian distribution with its mean and scatter estimated as follows. We first estimate σ_e using σ_{ap} through an empirical radial scaling:

$$\frac{\sigma_e}{\sigma_{\text{ap}}} = \frac{\langle \sigma_{\text{los}} \rangle (R = R_e)}{\langle \sigma_{\text{los}} \rangle (R = R_{\text{ap}})} = \left(\frac{R_e}{R_{\text{ap}}} \right)^\eta \quad (39)$$

where $\langle \sigma_{\text{los}} \rangle (R)$ is given by Equation (5) and we take $\eta = -[0.0392 + 0.0132(n - 4) - 0.0014(n - 4)^2]$, as appropriate for bulge-dominated galaxies (Bernardi et al. 2018b), with an rms scatter of 0.03. Then we estimate the mean value of w using Equation (35) with $a(K = 0)$ and its uncertainty by adding all uncertainties of parameters and coefficients quadratically (i.e., assuming normal errors). (We also assign a central black hole using the recent result (Saglia et al. 2016) and a central core as described in Chae, Bernardi & Kravtsov (2014), which are not however critical for our analysis, as $0.2R_e \lesssim R_{\text{ap}} \lesssim 1.2R_e$ for our selected SDSS galaxies.)

Given each set of (R_e, n, w) for the galaxy under consideration, we generate a trial random set of M_*/L gradient strength K , VD anisotropy $\beta(r)$, and DM halo parameters $(\log_{10} M_{200}, c_{\text{NFW}}, \alpha)$ under the Λ CDM paradigm. Here, $\log_{10} M_{200}$ and c_{NFW} are assigned using the empirical relations (Section 2.5), but α , K , and $\beta(r)$ are unknowns. For α we take a uniform deviate from the range $0 < \alpha < 1.8$ as in modeling the ATLAS^{3D} galaxies. For K we take a uniform deviate from the range $0 \leq K < K_{\text{max}}$. Based on the modeling results for the ATLAS^{3D} galaxies presented in §3.1 we choose $K_{\text{max}} = 1$ as our standard choice, and the median

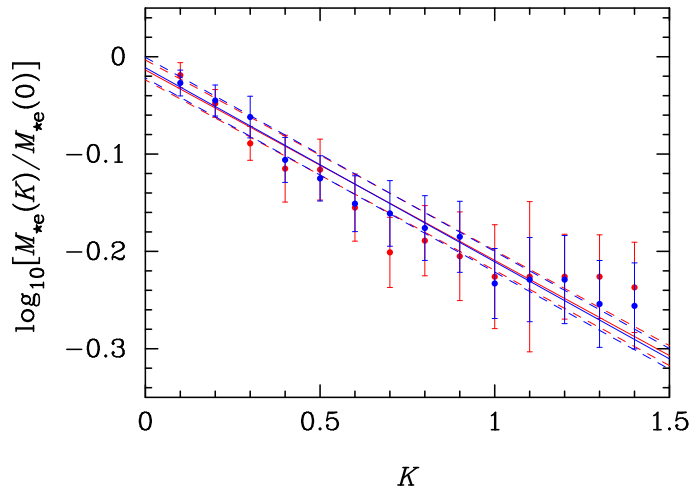


Fig. 18.— Same as Figure 17, but with respect to our own estimate of $M_{\star e}$ at $K = 0$. The fit results are as follows: $y = a' + b'K$ with $a' = -0.014 \pm 0.010$ and $b' = -0.20 \pm 0.02$ (red, best-fit), or $a' = -0.011 \pm 0.011$ and $b' = -0.20 \pm 0.02$ (blue, median).

becomes ≈ 0.5 . We consider varying K_{\max} from this standard value to estimate systematic uncertainties. Once a value of K is assigned, the stellar mass based on Equation (35) is shifted using Equation (37). For VD anisotropies we take the results of radially averaged values within R_e (Equation 38) for the 24 pure-bulge ATLAS^{3D} galaxies: $\langle \beta_e \rangle = 0.05 \pm 0.25$, which is consistent with the literature (Gerhard et al. 2001; Cappellari et al. 2007; Thomas et al. 2007). Specifically, we take a median from the range $-0.2 \leq \langle \beta_e \rangle \leq 0.3$ and take a Gaussian deviate of $\ln(\sigma_t^2/\sigma_r^2)_e = \ln(1 - \beta_e)$ with a median $\ln(1 - \langle \beta_e \rangle)$ and standard deviation of 0.5. We also consider radially varying anisotropies using the gOM model (Equation 3) with $r_a \leq R_e$ to study possible systematic uncertainties.

We then check if the aperture VD $\langle \sigma_{\text{los}} \rangle (R = R_{\text{ap}})$ (Equation 5) predicted for the trial set of parameters satisfies the measured SDSS VD σ_{ap} . If σ_{ap} is matched within the given error, the set is taken. If not, another set is tried and repeated up to a predefined maximum number of iterations $N_{\max}^{(1)} = 20$. If $\sigma(R_{\text{ap}})$ is still not matched within the formal error, we then check whether $\sigma(R_{\text{ap}})$ is matched within twice the formal error, iterating up to a larger maximum number $N_{\max}^{(2)} = 50$. After $N_{\max}^{(2)}$ iterations, any random set is taken. Even if larger values of $N_{\max}^{(1)}$ and $N_{\max}^{(2)}$ than these choices are considered, the results are little changed.

For the case of the MOND paradigm we use the general IF model given by Equation (11) and take for a_0 and ν uniform deviates, respectively, from (0.5, 1.9) in units of $10^{-10} \text{ m s}^{-2}$ and (0.1, 2), which encompass all likely possibilities.

Assuming normal errors of all the measured and derived quantities, we would expect 68% of the models in a Monte Carlo set to satisfy σ_{ap} within its uncertainty. We find that modeling with $K_{\max} = 0$ (no M_{\star}/L gradient) is successful in this sense for $\approx 89\%$ of galaxies. The success rate increases up to $\approx 99\%$ if the M_{\star}/L gradient ($K_{\max} > 0$) is considered. The failure rate of $\approx 1\% - 11\%$ is reasonable, as the spherical approximation may not be good for some of our galaxies. A range of results can be produced by varying K_{\max} and $\langle \beta_e \rangle$ from the above specified ranges, but, the results also depend on the scaling of dynamical

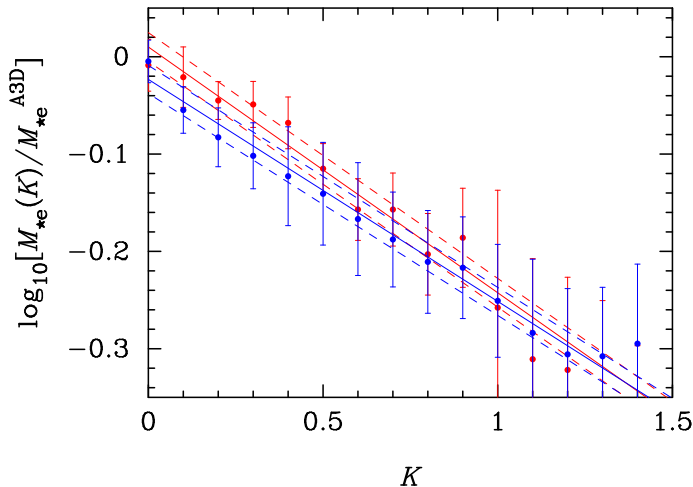


Fig. 19.— Same as Figure 17 but under the MOND paradigm. The fit results are as follows: $y = a' + b'K$ with $a' = 0.010 \pm 0.015$ and $b' = -0.25 \pm 0.03$ (red, best-fit), or $a' = -0.023 \pm 0.014$ and $b' = -0.23 \pm 0.03$ (blue, median).

stellar mass, or parameter b' in Equation 37, on K . For our SDSS galaxies this scaling is necessary because dynamical stellar masses are assigned using the FMP rather than determined by the observed VDPs, as for the ATLAS^{3D} galaxies. Thus, a Monte Carlo result is dictated primarily by the input choice of $(b', K_{\max}, \langle\beta_e\rangle)$. Based on the results for the ATLAS^{3D} galaxies shown in Figures 17 and 19, our standard choice of b' is -0.18 (the median result in Figure 17). We consider $b' = -0.16$ and -0.25 to estimate systematic uncertainties.

The Monte Carlo set of models produced for a given set of $(b', K_{\max}, \langle\beta_e\rangle)$ predicts a distribution of VP slope η (Equation 39) (see Chae & Gong (2015) for a previous example). We then check whether the prediction is consistent with the observed distribution of η from the similarly selected 24 pure-bulge ATLAS^{3D} galaxies: the mean $\langle\eta\rangle = -0.055 \pm 0.06$ and an rms scatter $s_\eta = 0.026$, which are derived by $\eta = \log(\sigma_e/\sigma_{e/8})/\log[R_e/(R_e/8)]$ taking the ATLAS^{3D} reported σ_e (Cappellari et al. 2013a) and $\sigma_{e/8}$ (Cappellari et al. 2013b) values. The required $\langle\beta_e\rangle$ to be consistent with $\langle\eta\rangle = -0.055 \pm 0.06$ depends on K_{\max} and b' . The stronger the K_{\max} or b' , the lower the $\langle\beta_e\rangle$. For $K_{\max} = 0$, $\langle\beta_e\rangle > 0$, but for $K_{\max} = 1$ or larger, $\langle\beta_e\rangle < 0$. For a given K_{\max} , $b' = -0.25$ requires a lower $\langle\beta_e\rangle$ compared with the standard choice $b' = -0.18$. For any choice of the set (b', K_{\max}) from $b' = [-0.25, -0.16]$ and $K_{\max} = [0, 1.5]$, respectively, there exists a value of $\langle\beta_e\rangle$ in the range $[-0.2, 0.3]$, so $\langle\eta\rangle = -0.055 \pm 0.06$ is matched within 2σ .

The large number of SDSS galaxies allows us to investigate scalings of various quantities with, e.g., stellar mass or VD. Figure 22 exhibits the distribution of the M_*/L gradient strength K with stellar mass and VD from the Monte Carlo sets with $K_{\max} = 1$ and 1.5 . The results indicate a correlation with stellar mass but not with VD. The correlation of K with $\log_{10}(M_*^{\text{Krou}}/M_\odot)$ depends on the assumed prior range of K . For $K_{\max} = 1$, we find a relatively weak but significant slope as $K = (0.503 \pm 0.002) + (0.087 \pm 0.023) [\log_{10}(M_*^{\text{Krou}}/M_\odot) - 11]$. For $K_{\max} = 1.5$, we have a stronger slope as $K = (0.700 \pm 0.002) + (0.224 \pm 0.008) [\log_{10}(M_*^{\text{Krou}}/M_\odot) - 11]$. Note here that SDSS data alone cannot prefer one over the other because K is not well constrained by the aperture VDs. However, the modeling results for the ATLAS^{3D} galaxies give $\langle K \rangle = 0.53^{+0.05}_{-0.04}$. Hence, a mild variation of K with stellar mass such as the results with $K_{\max} = 1$ is

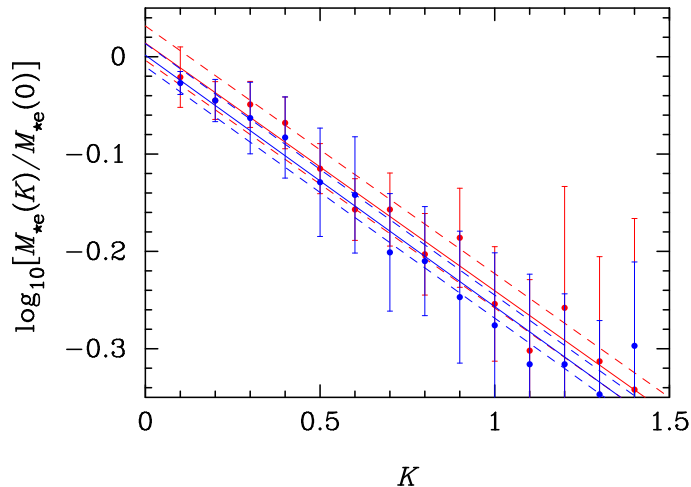


Fig. 20.— Same as Figure 19 but with respect to our own estimate of $M_{\star e}$ at $K = 0$. The fit results are as follows: $y = a' + b'K$ with $a' = 0.014 \pm 0.018$ and $b' = -0.25 \pm 0.03$ (red, best-fit), or $a' = 0.002 \pm 0.012$ and $b' = -0.26 \pm 0.03$ (blue, median).

more likely. A positive correlation such as this would be in qualitative agreement with Parikh et al. (2018).

4. Summary

We have considered nearly round pure-bulge galaxies (24 ATLAS^{3D} and 4201 SDSS galaxies) that are clearly distinct from rotating galaxies in structure and dynamics. We have carried out spherical Jeans modeling with radially varying VD anisotropies and radially varying M_{\star}/L gradients with multiple goals: (1) to provide constraints on theories of DM and gravity through radial acceleration relation, independent of rotating galaxies; and (2) to investigate the galactic structure of pure-bulges with the M_{\star}/L radial gradient. We have also presented simple analytical prescriptions to accommodate the M_{\star}/L radial gradient using the MGE and Sérsic light distributions.

For the ATLAS^{3D} galaxies the observed VD profiles are successfully reproduced with radially varying anisotropies (Equation 3) and a range of gradient strengths K (Equation 1). We have obtained Monte Carlo sets of models under both the Λ CDM and the MOND paradigms. Using these models we obtain the following results regarding dynamical stellar masses:

1. The FMP at fixed K is consistent with the virial expectation, i.e. dynamical stellar mass $M_{\star e} \propto \sigma_e^2 R_e$.
2. Dynamical stellar mass has the following scaling with K : $\log_{10} M_{\star e}(K) \approx \log_{10} M_{\star e}(K = 0) - 0.2K$.
3. The posterior distribution of K varies from galaxy to galaxy without a tendency for a universal value. The distribution has a median of $\langle K \rangle = 0.53^{+0.05}_{-0.04}$ and an rms scatter of $s_K = 0.17^{+0.06}_{-0.03}$. This is weaker than $K = 1$ (the van Dokkum et al. (2017) gradient), but in good agreement with the **Salp**^{In}–**Chab**^{Out} gradient $K = 0.555$ (Bernardi et al. 2018a).

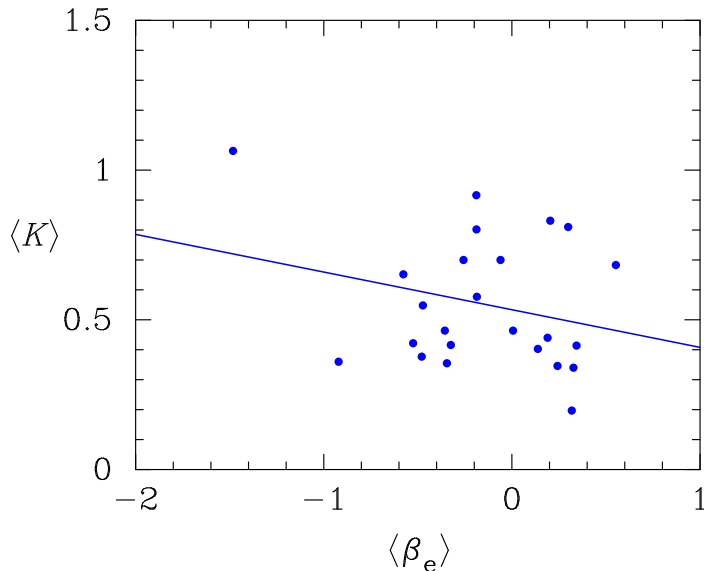


Fig. 21.— Anti-correlation between median M_*/L gradient strength, $\langle K \rangle$, and median VD anisotropy, $\langle \beta_e \rangle$, from the Monte Carlo sets of models of the ATLAS^{3D} galaxies.

4. From the above results on K and the scaling of the dynamical stellar mass with K (Equation 37), dynamical stellar masses, ignoring the M_*/L gradient are typically ≈ 0.1 dex overestimated.

We have also obtained Monte Carlo sets of models for the SDSS galaxies based on the accurate SDSS aperture VDs and the reliable FMP as a function of K derived for the ATLAS^{3D} galaxies. These Monte Carlo sets are useful for various statistical analyses, due to the large number of galaxies. From these sets we find:

1. There is an indication that M_*/L gradient has a positive correlation with stellar mass. The correlation starts to become significant if $\langle K \rangle \gtrsim 0.5$.

We use the Monte Carlo sets of models for the ATLAS^{3D} and SDSS galaxies obtained here to investigate the radial acceleration relation in Chae, Bernardi & Sheth (2018). Mass profiles, VD anisotropies, DM contents, or MOND IFs are analyzed in forthcoming papers.

Acknowledgments: We thank Michele Cappellari for useful communications regarding the ATLAS^{3D} data and modeling results. We also would like to thank the anonymous referee for the comments that helped us correct for errors and improve the presentation. This work was carried out at the University of Pennsylvania while K.-H.C. was on sabbatical leave. This research was supported by Basic Science Research Program through the National Research Foundation of Korea (NRF) funded by the Ministry of Education (NRF-2016R1D1A1B03935804).

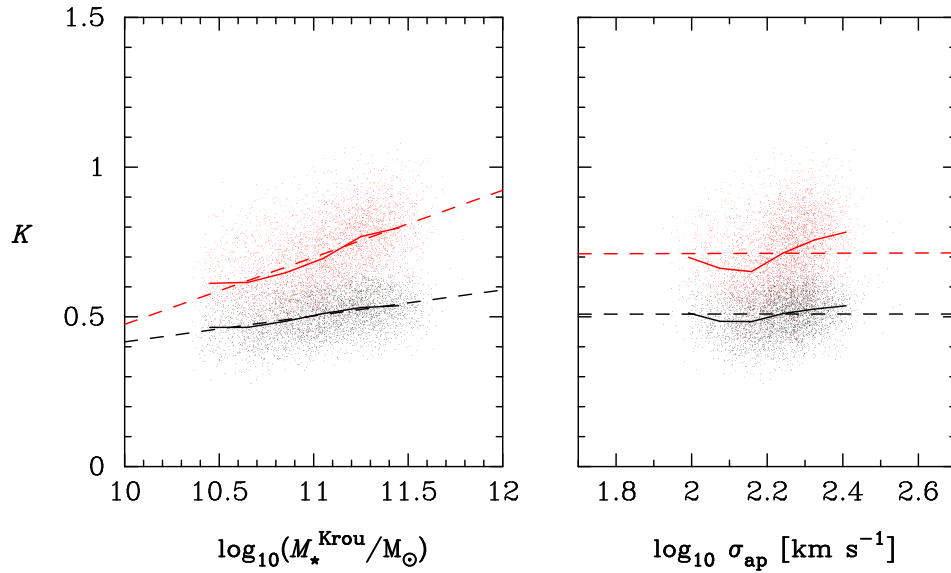


Fig. 22.— Posterior distribution of M_*/L gradient strength K with stellar mass M_*^{Krou} (mass based on the Kroupa IMF and $K = 0$) and SDSS aperture VD σ_{ap} from the Monte Carlo sets of models for ~ 4000 SDSS galaxies. The black and red points represent, respectively, the results with $K_{\text{max}} = 1$ and 1.5. The solid curves represent medians, while dashed lines are least-squares fit results. These results indicate a correlation of K with stellar mass but not with VD.

REFERENCES

- Abazajian, K. N., Adelman-McCarthy, J. K., Agüeros, M. A., et al. 2009, *ApJS*, 182, 543
- Bernardi, M., Sheth, R. K., Dominguez-Sanchez, H., et al. 2018a, *MNRAS*, 477, 2560
- Bernardi, M., Sheth, R. K., Fischer, J.-L., et al. 2018b, *MNRAS*, 475, 757
- Binney, J., Mamon, G. A. 1982, *MNRAS*, 200, 361
- Binney, J., Tremaine, S. 2008, *Galactic Dynamics*, (2nd ed.; Princeton, NJ: Princeton Univ. Press)
- Cappellari, M. 2016, *ARA&A*, 54, 597
- Cappellari, M., Emsellem, E., Bacon, R., et al. 2007, *MNRAS*, 379, 418
- Cappellari, M., Emsellem, E., Krajnović, D., et al. 2011, *MNRAS*, 413, 813
- Cappellari, M., Scott, N., Alatalo, K., et al. 2013a, *MNRAS*, 432, 1709
- Cappellari, M., McDermid, R. M., Alatalo, K., et al. 2013b, *MNRAS*, 432, 1862
- Chabrier, G. 2003, *PASP*, 115, 763
- Chae, K.-H., Bernardi, M., Kravtsov, A. V. 2014, *MNRAS*, 437, 3670
- Chae, K.-H., Bernardi, M., Sheth, R. K. 2018, *PhRvL*, submitted (arXiv:1707.08280v2)
- Chae, K.-H., Kravtsov, A. V., Frieman, J. A., Bernardi, M. 2012, *JCAP*, 11, 004
- Chae, K.-H., Gong, I.-T. 2015, *MNRAS*, 451, 1719
- Diemer, B., Kravtsov, A. V. 2015, *ApJ*, 799, 108
- Djorgovski, S., Davis, M. 1987, *ApJ*, 313, 59
- Dressler, A., Lynden-Bell, D., Burstein, D., et al. 1987, *ApJ*, 313, 42
- Emsellem, E., Monnet, G., & Bacon, R. 1994, *A&A*, 285, 723
- Emsellem, E., Cappellari, M., Krajnović, D., et al. 2011, *MNRAS*, 414, 888
- Famaey, B., Binney, J. 2005, *MNRAS*, 363, 603
- Famaey, B., Khoury, J., Penco, R. 2018, *JCAP*, 03, 038
- Famaey, B., McGaugh, S. S. 2012, *LRR*, 15, 10
- Gerhard, O., Kronawitter, A., Saglia, R. P., Bender, R. 2001, *AJ*, 121, 1936
- Huertas-Company, M., Aguerri, J. A. L., Bernardi, M., Mei, S., Sánchez Almeida, J. 2001, *A&A*, 525, 157
- Kent, S. M. 1987, *AJ*, 93, 816
- Krajnović, D., Alatalo, K., Blitz, L., et al. 2013, *MNRAS*, 432, 1768
- Kroupa, P. 2002, *Science*, 295, 82

- Lelli, F., McGaugh, S. S., Schombert, J. M., Pawlowski, M. S. 2017, *ApJ*, 836, 152
- Mandelbaum, R., Seljak, U., Hirata, C. M. 2008, *JCAP*, 08, 006
- Mandelbaum, R., Wang, W., Zu, Y., et al. 2016, *MNRAS*, 457, 3200
- Martín-Navarro, I., La Barbera, F., Vazdekis, A., Falcón-Barroso, J., Ferreras, I. 2015, *MNRAS*, 447, 1033
- Navarro, J. F., Frenk, C. S., White, S. D. M. 1997, *ApJ*, 490, 493
- McGaugh, S. S. 2004, *ApJ*, 609, 652
- McGaugh, S. S. 2005, *ApJ*, 632, 859
- McGaugh, S. S., Lelli, F., Schombert, J. M. 2016, *Phys. Rev. Lett.*, 117, 201101
- Meert, A., Vikram, V., Bernardi, M. 2013, *MNRAS*, 433, 1344
- Meert, A., Vikram, V., Bernardi, M. 2015, *MNRAS*, 446, 3943
- Merritt, D. 1985, *AJ*, 90, 1027
- Milgrom, M. 1983, *ApJ*, 270, 371
- Mo, H., van den Bosch, F. C., White, S. 2010, *Galaxy Formation and Evolution* (Cambridge: Cambridge Univ. Press)
- More, S., van den Bosch, F. C., Cacciato, M., Skibba, R., Mo, H. J., Yang, X. 2011, *MNRAS*, 410, 210
- Osipkov, L. P. 1979, *Pis'ma v Astron. Zhur.*, 5, 77
- Parikh, T., Thomas, D., Maraston, C., et al. 2018, *MNRAS*, 477, 3954
- Saglia, R. P., Opitsch, M., Erwin, P., et al. 2016, *ApJ*, 818, 47
- Salpeter, E. E. 1955, *ApJ*, 121, 161
- Scott, N., Cappellari, M., Davies, R. L., et al. 2013, *MNRAS*, 432, 1894
- Sérsic, J. L. 1968, *Atlas de Galaxias Australes* (Córdoba: Observatorio Astronómico)
- Sonnenfeld, A., Leauthaud, A., Auger, M. W., et al. 2018, *MNRAS*, submitted (arXiv:1801.01883)
- Thomas, D., Steele, O., Maraston, C., et al. 2013, *MNRAS*, 431, 1383
- Thomas, J., Saglia, R. P., Bender, R., et al. 2007, *MNRAS*, 382, 657
- van Dokkum, P., Conroy, C., Villaume, A., Brodie, J., Romanowsky, A. J. 2017, *ApJ*, 841, 68